

SUPPORTING INFORMATION TO THE MANUSCRIPT

Integrated Molecular, Morphological and Interfacial Engineering towards High-Performance and Stable Solution-processed Small Molecule Solar Cells

Jie Min*^{1†}, Yuriy N. Luponosov*^{2†}, Nicola Gasparini¹, Lingwei Xue³, Fedor V. Drozdov², Svetlana M. Peregudova⁴, Petr V. Dmitryakov⁵, Kirill L. Gerasimov⁶, Denis V. Anokhin^{6,7}, Zhi-Guo Zhang³, Tayebbeh Ameri¹, Sergei N. Chvalun^{2,5}, Dimitri A. Ivanov^{6,8}, Yongfang Li³, Sergei A. Ponomarenko^{2,9}, and Christoph J. Brabec^{1,10}

¹Institute of Materials for Electronics and Energy Technology (I-MEET), Friedrich-Alexander-University Erlangen-Nuremberg, Martensstraße 7, 91058 Erlangen, Germany

²Enikolopov Institute of Synthetic Polymeric Materials of the Russian Academy of Sciences, Profsoyuznaya St. 70, Moscow 117393, Russia

³CAS Key Laboratory of Organic Solids, Institute of Chemistry, Chinese Academy of Sciences, Beijing 100190, China

⁴Nesmeyanov Institute of Organoelement Compounds, Russian Academy of Sciences, Vavilova St. 28, Moscow, 119991, Russia

⁵National Research Centre "Kurchatov Institute", 1, Akademika Kurchatova pl., Moscow, 123182, Russia

⁶Moscow State University, Faculty of Fundamental Physical and Chemical Engineering, GSP-1, 1-51 Leninskie Gory, Moscow, 119991, Russia;

⁷Institute for Problems of Chemical Physics, Russian Academy of Sciences, Semenov Prospect 1, Chernogolovka, Moscow Region, 142432, Russia

⁸Institut de Sciences des Matériaux de Mulhouse (CNRS UMR7361), 15 rue Jean Starcky, B.P 2488, Mulhouse, 68057, France

⁹Chemistry Department, Moscow State University, Leninskie Gory 1-3, Moscow 119991, Russia

¹⁰Bavarian Center for Applied Energy Research (ZAE Bayern), Haberstraße 2a, 91058 Erlangen, Germany

† These two first authors contributed equally

*E-mail: Min.Jie@ww.uni-erlangen.de (J. Min); luponosov@ispm.ru (Y.N. Luponosov)

CONTENTS

1. Experimental Section	3
1.1. General.....	3
1.2. Materials and Synthetic procedures.....	4
1.3 Fabrication and characterization of the OSCs.....	9
2. Results and discussion	11
2.1 ¹ H NMR and ¹³ C NMR spectra.....	11
2.2 Thermal properties of the DTS-based oligomers.....	21
2.3 Optical and electrochemical properties of oligomers.....	22
2.4 Photovoltaic properties of the DTS-based oligomers	24
2.5 Morphology Characterizations and investigations.....	26
2.6 Charge transport properties and recombination dynamics.....	31
References	40

1. Experimental Section

1.1 General.

Characterization of precursors and oligomers. ^1H NMR spectra were recorded at a “Bruker WP-250 SY” spectrometer, working at a frequency of 250.13 MHz and utilising CDCl_3 signal (7.25 ppm) as the internal standard. ^{13}C NMR spectra were recorded using a “Bruker Avance II 300” spectrometer at 75 MHz and Bruker DRX500 at 125 MHz. In the case of ^{13}C NMR spectroscopy, the compounds to be analysed were taken in the form of $\approx 5\%$ solutions in CDCl_3 . The spectra were then processed on the computer using the ACD Labs software. Mass-spectra (MALDI) were registered on the Autoflex II Bruker (resolution FWHM 18000), equipped with a nitrogen laser (work wavelength 337 nm) and time-of-flight mass-detector working in reflections mode. The accelerating voltage was 20 kV. Samples were applied to a polished stainless steel substrate. Spectrum was recorded in the positive ion mode. The resulting spectrum was the sum of 300 spectra obtained at different points of sample. 2,5-dihydroxybenzoic acid (DHB) (Acros, 99%) and α -cyano-4-hydroxycinnamic acid (HCCA) (Acros, 99%) were used as matrices. Elemental analysis of C, H, N elements was carried out using CHN automatic analyzer CE 1106 (Italy). The settling titration using BaCl_2 was applied to analyze sulphur. Spectrophotometry technique was used for the Si analysis. Experimental error is 0.30-0.50%. The Knövenagel condensation was carried out in the microwave “Discovery”, (CEM corporation, USA), using a standard method with the open vessel option, 50 watts.

Thermal properties characterization. Thermogravimetric analysis was carried out in dynamic mode in $30 \div 900^\circ\text{C}$ interval using Mettler Toledo TG50 system equipped with M3 microbalance allowing measuring the weight of samples in 0 - 150 mg range with 1 μg precision. Heating/cooling rate was chosen to be $10^\circ\text{C}/\text{min}$. Every compound was studied twice: in air and in nitrogen flow of 200 mL/min. DSC scans were obtained with Mettler Toledo DSC30 system with $10^\circ\text{C}/\text{min}$ heating/cooling rate in temperature range of $+20 \div 290^\circ\text{C}$ for all compounds. N_2 flow of 50 mL/min was used.

Cyclic voltammetry (CV) measurements were carried out using solid compact layers of the oligomers, which in turn were made by electrostatically rubbing the materials onto a glassy carbon electrode using IPC-Pro M potentiostat. Measurements were made in acetonitrile solution using 0.1 M Bu_4NPF_6 as supporting electrolyte. The scan rate was 200 mV s^{-1} . The glassy carbon electrode was used as a work electrode. Potentials were measured relative to a saturated calomel electrode (SCE). Solution CV measurements were done in 1,2-dichlorobenzene/acetonitrile (4:1) mixture of solvents for 10^{-3}M solutions in a standard three-electrode cell equipped with a glassy carbon working electrode ($s=2 \text{ mm}^2$), platinum plate as the counter electrode, and SCE (saturated calomel electrode) as the reference electrode. The highest occupied molecular orbital (HOMO) and the

lowest unoccupied molecular orbital (LUMO) energy levels were calculated using the first standard formal oxidation and reduction potentials obtained from CV experiments in films according to following equation: $LUMO = e(\varphi_{red} + 4.40)(eV)$ and $HOMO = -e(\varphi_{ox} + 4.40)(eV)$.^[1]

Solubility's measurement. Saturated solutions of molecules in chloroform were prepared by stirring of excess of solid material in the solvent. For this purpose, small molecules were added in small portions to ca. 1 mL of pure solvent. When this first portion of the materials was completely dissolved, additional small portions were added to the stirred solution one after the other until some solid remained undissolved. As prepared saturated solution were filtered through 0.25- μ m PTFE syringe filters into glass bottles. Immediately after filtration the solution was quickly and quantitatively transferred (500 μ L) into another glass bottles of known mass, and then left on a hot place (60 °C) to facilitate solvent evaporation. Usually 1 h was sufficiently long to evaporate 500 μ L of chloroform and reach constant weight for the glass bottles with the solid residue. The mass of dissolved materials in 500 μ L of chloroform was assumed as being equivalent to the difference between the weight of an empty bottle and the same bottle with a solid residue after solvent evaporation. After that, we could calculate the solubility of relevant material. This solvation effect results in an overestimation of the solubility by 10%. Note that the effect of solvate formation was neglected in our solubility estimations.

Absorption profiles were recorded with a Perkin Elmer Lambda-35 absorption spectrometer from 350 to 1100 nm.

AFM measurements were performed with a Nanosurf Easy Scan 2 in contact mode.

Grazing-Incidence Wide-Angle X-ray Scattering (GIWAXS) measurements were performed using XeuSS SAXS/WAXS (Xenocs, France) diffractometer coupled to a GeniX3D generator ($\lambda = 1.54$ Å). The 2D patterns were collected with the incidence angle of 0.2° using Rayonix HS170 CCD detector (pixel size 132x132 μ m) with sample-to-detector distance of approximately 18cm. The modulus of the scattering vector s ($s = 2\sin\theta/\lambda$, where θ is the Bragg angle) was calibrated using seven diffraction orders of silver behenate. After background subtraction and noise correction, indexing of 2D-GIWAXS patterns was performed with a home-made routine designed in Igor Pro software (Wavemetrics Ltd.).

1.2 Materials and Synthetic procedures.

n-Butyl lithium (1.6 M solution in hexane), magnesium, isopropoxy-4,4,5,5-tetramethyl-1,3,2-dioxaborolane (IPTMDOB), tetrakis(triphenylphosphine)palladium (0) Pd(PPh₃)₄, p-toluenesulfonic acid (p-TosH), malononitile, heptanoyl chloride, propanoyl chloride 2,2'-bithiophene, 2-bromothiophene, 2,2-dimethyl-1,3-propanediol were obtained from Sigma–Aldrich Co. and used without further purification. THF, benzene and pyridine were dried and purified according to the known techniques and then used as solvents. Synthesis of DTS(Oct)₂-(2T-DCV-Me)₂^[1] and

DTS(Oct)₂-(2T-DCV-Hex)₂^[2] described elsewhere. 4,4'-bis(octyl)-5,5'-dibromo-dithieno[3,2-*b*:2',3'-*d*]silole (**4e**),^[3] 4,4'-bis(2-ethylhexyl)-5,5'-dibromo-dithieno[3,2-*b*:2',3'-*d*]silole^[4] (**4f**) and 4,4'-bis(2-decyl)-5,5'-dibromo-dithieno[3,2-*b*:2',3'-*d*]silole (**4g**) were obtained as described elsewhere^[5]. The synthesis of compounds 1b-d was described earlier.^[1, 6, 7], while preparation of **1a** will be published elsewhere.^[8] All reactions, unless stated otherwise, were carried out under an inert atmosphere.

2,6-bis[5'-(5,5-dimethyl-1,3-dioxan-2-yl)-2,2'-bithien-5-yl]-4,4-dioctyl-4*H*-silolo[3,2-*b*:4,5-*b'*]dithiophene (3ae**)**. In the inert atmosphere, degassed solutions of **1a** (1.86 g, 4.6 mmol) and 4,4'-bis(octyl)-5,5'-dibromo-dithieno[3,2-*b*:2',3'-*d*]silole (**2e**) (1.08 g, 1.9 mmol) in toluene/ethanol mixture (50/8 mL) and 2M solution of aq. Na₂CO₃ (7 mL) were added to Pd(PPh₃)₄ (185 mg, 0.16 mmol). The reaction mixture was stirred under reflux for 10 h, and then it was cooled to room temperature and poured into 75 mL of water and 100 mL of toluene. The organic phase was separated, washed with water, dried over sodium sulfate and filtered. The solvent was evaporated in vacuum and the residue was dried at 1 Torr. The product was purified by column chromatography on silica gel (eluent toluene) to give pure compound **3ae** (1.59 g, 87%) as a dark-red solid. ¹H NMR (250 MHz, CDCl₃): δ [ppm] 0.80 (s, 6H), 0.84 (t, 6H, *J* = 6.7 Hz), 0.92 (m, M = 5, 4H, *J* = 6.7 Hz), 1.20–1.31 (24H, overlapping peaks), 1.33–1.43 (broadened signal, 4H), 3.62 (d, 4H, *J* = 11 Hz), 3.74 (d, 4H, *J* = 11 Hz), 5.61 (s, 2H), 6.99–7.09 (8H, overlapping peaks), 7.10 (s, 2H). ¹³C NMR (125 MHz, CDCl₃): δ [ppm] 11.73, 14.10, 21.81, 22.66, 22.94, 24.11, 29.12, 29.22, 30.20, 31.85, 33.15, 77.50, 98.08, 122.93, 123.83, 124.49, 125.80, 126.39, 136.56, 137.44, 137.46, 140.12, 143.05, 144.64, 147.74. Calcd (%) for C₅₂H₆₆O₄S₆Si: C, 64.02; H, 6.82; S, 19.72; Si, 2.88. Found: C, 64.06; H, 6.83; S, 19.68; Si, 2.86. MALDI-MS: found *m/z* 974.31; calculated for [M]⁺ 974.05.

5',5''-(4,4-dioctyl-4*H*-silolo[3,2-*b*:4,5-*b'*]dithiophene-2,6-diyl)bis(2,2'-bithiophene-5-carbaldehyde) (4ae**)**. 1M HCl (1.4 mL) was added to a solution of compound **3ae** (0.85 g, 0.87 mmol) in THF (15 mL), and then the reaction mixture was stirred for 4 hours at reflux. During the reaction the product was gradually formed as orange precipitate. After completion of the reaction the organic phase was separated using diethyl ether, washed with water and filtered off to give crude product on the filter containing about 5% of initial 5,5-dimethyl-1,3-dioxan groups. Therefore, the reaction sequence was repeated one more time, in order to remove the rest of protective groups, to give on the filter pure compound **4ae** (0.66 g, 95%) as a dark-red solid. ¹H NMR (250 MHz, CDCl₃): δ [ppm] 0.84 (t, 6H, *J* = 6.7 Hz), 0.95 (m, M = 5, 4H, *J* = 6.7 Hz), 1.19–1.45 (24H, overlapping peaks), 7.09 (d, 2H, *J* = 3.7 Hz), 7.18 (s, 2H), 7.21 (d, 2H, *J* = 3.7 Hz), 7.26 (d, 2H, *J* = 3.7 Hz), 7.66 (d, 2H, *J* = 3.7 Hz), 9.35 (s, 2H). Calcd (%) for C₄₂H₄₆O₂S₆Si: C, 62.80; H, 5.77; S, 23.95; Si, 3.50. Found: C, 62.83; H, 5.78; S, 23.90; Si, 3.46. MALDI-MS: found *m/z* 802.16; calculated for [M]⁺ 801.95.

2,2'-[(4,4-dioctyl-4*H*-silolo[3,2-*b*:4,5-*b'*]dithiophene-2,6-diyl)bis(2,2'-bithiene-5',5-diylmethylidene)]dimalononitrile (DTS(Oct)₂-(2T-DCV)₂). Compound **4ae** (0.5 g, 0.6 mmol), malononitrile (0.25 g, 3.7 mmol) and dry pyridine (10 mL) were placed in a reaction vessel and stirred under argon atmosphere for 8 hours at 107 °C using the microwave heating. After completeness of the reaction the pyridine was evaporated in vacuum and the residue was dried at 1 Torr. This crude product was purified by column chromatography on silica gel (eluent dichloromethane) to give pure product as a black solid (0.46 g, 83 %). M.p.: 259 °C. ¹H NMR (250 MHz, CDCl₃): δ [ppm] 0.84 (t, 6H, *J* = 6.7 Hz), 0.95 (m, M = 5, 4H, *J* = 6.7 Hz), 1.22–1.41 (24H, overlapping peaks), 7.13 (d, 2H, *J* = 3.7 Hz), 7.21–7.24 (4H, overlapping peaks), 7.35 (d, 2H, *J* = 3.7 Hz), 7.62 (d, 2H, *J* = 3.7 Hz), 7.74 (s, 2H). Calcd (%) for C₄₈H₄₆N₄S₆Si: C, 64.10; H, 5.16; N, 6.23; S, 21.39; Si, 3.12%. Found: C, 64.16; H, 5.18; N, 6.22; S, 21.34; Si, 3.08%. MALDI MS: found *m/z* 898.18; calculated for [M]⁺ 897.94.

2,6-bis[5'-(2-ethyl-5,5-dimethyl-1,3-dioxan-2-yl)-2,2'-bithien-5-yl]-4,4-dioctyl-4*H*-silolo[3,2-*b*:4,5-*b'*]dithiophene (3ce). This compound was obtained by the method described above for compound **3ae** using compound **1c** (1.04 g, 2.4 mmol), and **2e** (0.57 g, 1.0 mmol), Pd(PPh₃)₄ (138 mg, 0.12 mmol) and aq. 2M Na₂CO₃ (4.25 mL). The crude product was purified by column chromatography on silica gel (eluent toluene) to give pure compound **3ce** (0.82 g, 82%) as a red solid. M.p.: 203 °C. ¹H NMR (250 MHz, CDCl₃): δ [ppm] 0.66 (s, 6H), 0.85 (t, 6H, *J* = 6.7 Hz), 0.94 (t, 6H, *J* = 6.7 Hz), 1.19–1.30 (24H, overlapping peaks with maximum at 1.23 ppm), 1.35–1.46 (broadened signal, 4H), 1.88 (m, M = 4, 4H, *J* = 7.3 Hz), 3.41 (d, 2H, *J* = 11 Hz), 3.71 (d, 2H, *J* = 11 Hz), 6.86 (d, 2H, *J* = 3.7 Hz), 7.02–7.08 (overlapping peaks, 6H), 7.12 (s, 2H). ¹³C NMR (125 MHz, CDCl₃): δ [ppm] 7.62, 11.75, 14.07, 21.90, 22.64, 22.74, 24.12, 29.11, 29.20, 29.83, 31.83, 33.14, 37.71, 71.88, 100.50, 123.12, 123.81, 124.16, 126.34, 127.05, 135.73, 136.32, 137.36, 137.94, 143.16, 143.37, 147.70. Calcd (%) for C₅₆H₇₄O₄S₆Si: C, 65.20; H, 7.23; S, 18.65; Si, 2.72. Found: C, 65.24; H, 7.21; S, 18.60; Si, 2.70. MALDI-MS: found *m/z* 1030.10; calculated for [M]⁺ 1030.37.

1,1'-[(4,4-dioctyl-4*H*-silolo[3,2-*b*:4,5-*b'*]dithiophene-2,6-diyl)bis(2,2'-bithiene-5',5-diyl)]dipropan-1-one (4ce). This compound was obtained by the method described above for compound **4ae** using compound **3ce** (0.62 g, 0.06 mmol), 1M HCl (1.50 mL) and THF (7 mL). After the completeness of the reaction the organic phase was separated, washed with water and filtered off to give pure product (0.81 g, 97%) as a red solid. ¹H NMR (250 MHz, CDCl₃): δ [ppm] 0.85 (t, 6H, *J* = 6.7 Hz), 0.94 (m, M = 5, 4H, *J* = 6.7 Hz), 1.22–1.42 (30H, overlapping peaks), 2.90 (m, M = 4, 4H, *J* = 7.3 Hz), 7.07 (d, 2H, *J* = 3.7 Hz), 7.12 (d, 2H, *J* = 3.7 Hz), 7.16 (s, 2H), 7.21 (d, 2H, *J* = 3.7 Hz), 7.59 (d, 2H, *J* = 3.7 Hz). Calcd (%) for C₄₆H₅₄O₂S₆Si: C, 64.29; H, 6.33; S, 22.39;

Si, 3.27. Found: C, 64.25; H, 6.30; S, 22.32; Si, 3.24. MALDI MS: found m/z 858.00; calculated for $[M]^+$ 858.22.

2,2'-[(4,4-dioctyl-4H-silolo[3,2-*b*:4,5-*b'*]dithiophene-2,6-diyl)bis(2,2'-bithiene-5',5'-diylprop-1-yl-1-ylidene)]dimalononitrile (DTS(Oct)₂-(2T-DCV-Et)₂). This compound was obtained by the method described above for **DTS(Oct)₂-(2T-DCV)₂** using compound **4ce** (0.46 g, 0.53 mmol) and malononitrile (0.21 g, 3.2 mmol). The crude product was purified by column chromatography on silica gel (eluent dichloromethane:toluene, 1:1). Further purification included precipitation of the product from its THF solution with toluene and hexane to give pure product as a black solid (0.46 g, 89%). M.p.: 203 °C. ¹H NMR (250 MHz, CDCl₃): δ [ppm] 0.84 (t, 6H, $J = 6.7$ Hz), 0.96 (m, M=5, 4H, $J = 6.7$ Hz), 1.20–1.42 (30H, overlapping peaks), 2.95 (m, M = 5, 4H, $J = 6.7$ Hz), 7.11 (d, 2H, $J = 3.7$ Hz), 7.20 (s, 2H), 7.24 (d, 2H, $J = 4.3$ Hz), 7.28 (d, 2H, $J = 3.7$ Hz), 7.96 (d, 2H, $J = 4.3$ Hz). ¹³C NMR (75 MHz, CDCl₃): δ [ppm] 11.83, 14.01, 22.65, 23.05, 24.17, 29.14, 29.20, 31.86, 33.11, 113.88, 114.45, 124.47, 124.69, 127.51, 133.35, 135.16, 136.02, 137.69, 140.08, 144.18, 146.56, 148.72, 160.76. ²⁹Si NMR (60 MHz, CDCl₃, δ , ppm): -3.71. Calcd (%) for C₅₂H₅₄N₄S₆Si: C, 65.37; H, 5.70; N, 5.86; S, 20.13; Si, 2.94%. Found: C, 65.41; H, 5.72; N, 5.84; S, 20.09; Si, 2.90%. MALDI MS: found m/z 953.88; calculated for $[M]^+$ 954.24.

2,6-bis[5'-(2-methyl-5,5-dimethyl-1,3-dioxan-2-yl)-2,2'-bithien-5-yl]-4,4-bis(2-ethylhexyl)-4H-silolo[3,2-*b*:4,5-*b'*]dithiophene (3bf). This compound was obtained by the method described above for compound **3ae** using compound **1b** (1.41 g, 3.3 mmol), and **2f** (0.75 g, 1.3 mmol), Pd(PPh₃)₄ (190 mg, 0.16 mmol) and aq. 2M Na₂CO₃ (4.8 mL). The crude product was purified by column chromatography on silica gel (eluent toluene:hexane, 1:1) to give pure compound **3bf** (1.07 g, 82%) as a red solid. ¹H NMR (250 MHz, CDCl₃): δ [ppm] 0.68 (s, 6H), 0.75–0.87 (12H, overlapping peaks), 0.97 (m, M = 5, 4H, $J = 6.7$ Hz), 1.15–1.31 (22H, overlapping peaks with maximum at 1.23 ppm), 1.44 (m, M = 4, 2H, $J = 6.7$ Hz), 1.69 (s, 6H), 3.41 (d, 2H, $J = 11$ Hz), 3.70 (d, 2H, $J = 11$ Hz), 6.90 (d, 2H, $J = 3.7$ Hz), 7.03 (d, 2H, $J = 3.7$ Hz), 7.04–7.07 (overlapping peaks, 4H), 7.11 (s, 2H). ¹³C NMR (125 MHz, CDCl₃): δ [ppm] 10.81, 14.16, 21.28, 21.89, 22.64, 22.99, 26.48, 28.86, 28.93, 29.75, 35.63, 35.91, 72.00, 98.60, 123.28, 124.10, 126.34, 127.16, 133.40, 134.36, 137.57, 138.71, 142.21, 143.51, 145.48, 147.93. Calcd (%) for C₅₄H₇₀O₄S₆Si: C, 64.63; H, 7.03; S, 19.17; Si, 2.80. Found: C, 64.74; H, 7.06; S, 19.05; Si, 2.74. MALDI-MS: found m/z 1001.99; calculated for $[M]^+$ 1002.34.

2,6-bis(5'-acetyl-2,2'-bithien-5-yl)-4,4-bis(2-ethylhexyl)-4H-silolo[3,2-*b*:4,5-*b'*]dithiophene (4bf). This compound was obtained by the method described above for compound **4ae** using compound **3bf** (0.65 g, 0.07 mmol), 1M HCl (2.50 mL) and THF (13 mL). After the completeness of the reaction the organic phase was separated, washed with water and filtered off to give pure product (0.51 g, 95%) as a red solid. ¹H NMR (250 MHz, CDCl₃): δ [ppm] 0.79 (t, 6H, $J = 6.7$ Hz),

0.83 (t, 6H, $J=6.7$ Hz), 0.94-1.03 (4H, broadened signal), 1.14–1.31 (16H, overlapping peaks), 1.44 (m, $M=4$, 2H, $J=6.7$ Hz), 2.55 (s, 6H), 7.07 (d, 2H, $J=3.7$ Hz), 7.14 (d, 2H, $J=3.7$ Hz), 7.16 (s, 2H), 7.22 (d, 2H, $J=3.7$ Hz), 7.58 (d, 2H, $J=3.7$ Hz). Calcd (%) for $C_{44}H_{50}O_2S_6Si$: C, 65.56; H, 6.57; S, 22.58; Si, 2.47. Found: C, 65.61; H, 6.59; S, 22.46; Si, 2.43. MALDI MS: found m/z 829.90; calculated for $[M]^+$ 830.19.

2,2'-[(4,4-bis(2-ethylhexyl)-4H-silolo[3,2-*b*:4,5-*b'*]dithiophene-2,6-diyl)bis(2,2'-bithiene-5',5-diylprop-1-yl-1-ylidene)]dimalononitrile (DTS(EtHex)₂-(2T-DCV-Me)₂). This compound was obtained by the method described above for **DTS(Oct)₂-(2T-DCV)₂** using compound **4bf** (0.50 g, 0.6 mmol) and malononitrile (0.23 g, 3.6 mmol). The crude product was purified by column chromatography on silica gel (eluent dichloromethane:toluene, 1:1). Further purification included precipitation of the product from its THF solution with toluene and hexane to give pure product as a black solid (0.49 g, 87%). M.p.: 230 °C. ¹H NMR (250 MHz, CDCl₃): δ [ppm] 0.80 (t, 6H, $J=6.7$ Hz), 0.83 (t, 6H, $J=6.7$ Hz), 0.98 (m, $M=5$, 4H, $J=6.7$ Hz), 1.13–1.34 (16H, overlapping peaks), 1.45 (m, $M=4$, 2H, $J=6.7$ Hz), 2.67 (s, 6H), 7.08 (d, 2H, $J=3.7$ Hz), 7.18 (s, 2H), 7.23 (d, 2H, $J=4.3$ Hz), 7.27 (d, 2H, $J=3.7$ Hz), 7.94 (d, 2H, $J=4.3$ Hz). ¹³C NMR (75 MHz, CDCl₃): δ [ppm] 11.83, 14.01, 22.65, 23.05, 24.17, 29.14, 29.20, 31.86, 33.11, 113.88, 114.45, 124.47, 124.69, 127.51, 133.35, 135.16, 136.02, 137.69, 140.08, 144.18, 146.56, 148.72, 160.76. Calcd (%) for $C_{50}H_{50}N_4S_6Si$: C, 64.75; H, 5.43; N, 6.04; S, 20.74; Si, 3.03%. Found: C, 64.81; H, 5.46; N, 6.00; S, 20.68; Si, 3.00%. MALDI MS: found m/z 926.21; calculated for $[M]^+$ 925.88.

2,6-bis[5'-(2-decyl-5,5-dimethyl-1,3-dioxan-2-yl)-2,2'-bithien-5-yl]-4,4-dioctyl-4H-silolo[3,2-*b*:4,5-*b'*]dithiophene (3bg). This compound was obtained by the method described above for compound **3ae** using compound **1b** (1.15 g, 2.8 mmol), and **2g** (0.72 g, 1.1 mmol), Pd(PPh₃)₄ (160 mg, 0.1 mmol) and aq. 2M Na₂CO₃ (4.10 mL). The crude product was purified by column chromatography on silica gel (eluent toluene:hexane, 1:1) to give pure compound **3bg** (1.02 g, 84%) as a red solid. ¹H NMR (250 MHz, CDCl₃): δ [ppm] 0.68 (s, 6H), 0.84 (t, 6H, $J=6.7$ Hz), 0.92 (m, $M=5$, 4H, $J=6.7$ Hz), 1.17–1.35 (34H, overlapping peaks with maximum at 1.22 ppm), 1.35-1.48 (broadened signal, 4H), 1.69 (s, 6H), 3.41 (d, 2H, $J=11$ Hz), 3.70 (d, 2H, $J=11$ Hz), 6.90 (d, 2H, $J=3.7$ Hz), 7.03 (d, 2H, $J=3.7$ Hz), 7.04–7.06 (overlapping peaks, 4H), 7.12 (s, 2H). ¹³C NMR (125 MHz, CDCl₃): δ [ppm] 11.70, 14.11, 21.27, 22.62, 22.68, 24.10, 26.65, 29.16, 29.34, 29.56, 29.61, 31.89, 33.12, 36.48, 71.87, 98.57, 124.10, 125.61, 126.48, 128.22, 135.65, 136.40, 137.63, 138.62, 143.62, 145.47, 148.18. Calcd (%) for $C_{58}H_{78}O_4S_6Si$: C, 65.74; H, 7.42; S, 18.15; Si, 2.65. Found: C, 65.80; H, 7.45; S, 18.07; Si, 2.61. MALDI-MS: found m/z 1058.13; calculated for $[M]^+$ 1058.40.

1,1'-[(4,4-didecyl-4H-silolo[3,2-*b*:4,5-*b'*]dithiophene-2,6-diyl)bis(2,2'-bithiene-5',5-diyl)]dipropan-1-one (4bg). This compound was obtained by the method described above for compound **4ae** using compound **3bg** (0.7 g, 0.7 mmol), 1M HCl (1.50 mL) and THF (10 mL). After

the completeness of the reaction the organic phase was separated, washed with water and filtered off to give pure product (0.56 g, 95%) as a red solid. ^1H NMR (250 MHz, CDCl_3): δ [ppm] 0.85 (t, 6H, $J = 6.7$ Hz), 0.94 (m, M = 5, 4H, $J = 6.7$ Hz), 1.21–1.46 (32H, overlapping peaks), 2.54 (s, 6H), 7.07 (d, 2H, $J = 3.7$ Hz), 7.13 (d, 2H, $J = 3.7$ Hz), 7.16 (s, 2H), 7.21 (d, 2H, $J = 3.7$ Hz), 7.57 (d, 2H, $J = 3.7$ Hz). Calcd (%) for $\text{C}_{48}\text{H}_{58}\text{O}_2\text{S}_6\text{Si}$: C, 64.96; H, 6.59; S, 21.68; Si, 3.16. Found: C, 64.91; H, 6.56; S, 21.60; Si, 3.12. MALDI-MS: found m/z 886.01; calculated for $[\text{M}]^+$ 886.25.

2,2'-[(4,4-didecyl-4*H*-silolo[3,2-*b*:4,5-*b'*]dithiophene-2,6-diyl)bis(2,2'-bithiene-5',5'-diylprop-1-yl-1-ylidene)]dimalononitrile (DTS(Dec)₂-(2T-DCV-Me)₂). This compound was obtained by the method described above for **DTS(Oct)₂-(2T-DCV)₂** using compound **4bg** (0.45 g, 0.51 mmol) and malononitrile (0.20 g, 3.0 mmol). The crude product was purified by column chromatography on silica gel (eluent dichloromethane:toluene, 1:1). Further purification included precipitation of the product from its THF solution with toluene and hexane to give pure product as a black solid (0.45 g, 90%). M.p.: 205 °C. ^1H NMR (250 MHz, CDCl_3): δ [ppm] 0.86 (t, 6H, $J = 6.7$ Hz), 0.96 (m, M = 5, 4H, $J = 6.7$ Hz), 1.21–1.45 (32H, overlapping peaks), 2.66 (s, 6H), 7.10 (d, 2H, $J = 3.7$ Hz), 7.19 (s, 2H), 7.23 (d, 2H, $J = 4.3$ Hz), 7.27 (d, 2H, $J = 3.7$ Hz), 7.94 (d, 2H, $J = 4.3$ Hz). ^{13}C NMR (75 MHz, CDCl_3): δ [ppm] 11.66, 14.10, 22.67, 22.99, 24.14, 29.18, 29.35, 29.57, 29.61, 31.89, 33.15, 113.98, 114.53, 124.28, 124.52, 127.36, 127.49, 133.08, 135.37, 135.69, 137.61, 139.94, 143.94, 146.56, 148.57, 160.78. Calcd (%) for $\text{C}_{54}\text{H}_{58}\text{N}_4\text{S}_6\text{Si}$: C, 65.94; H, 5.94; N, 5.70; S, 19.56; Si, 2.86%. Found: C, 65.89; H, 5.90; N, 5.68; S, 19.49; Si, 2.82%. MALDI MS: found m/z 982.29; calculated for $[\text{M}]^+$ 981.98.

1.3 Fabrication and characterization of the OSCs

The conventional photovoltaic devices were processed and characterized in air. Pre-structured ITO coated glass substrates were subsequently cleaned in acetone and isopropyl alcohol for 10 min each. After drying, the substrates were coated via doctor blading with 40 nm PEDOT:PSS (Heraeus, Clevios P VP.Al 4083). The concentration of the active layer solutions is about 14 mg mL⁻¹. Among these oligomers, DTS(Oct)₂-(2T-DCV-Et)₂, DTS(Oct)₂-(2T-DCV-Hex)₂, DTS(EtHex)₂-(2T-DCV-Me)₂ and DTS(Dec)₂-(2T-DCV-Me)₂ based active layers (80-100 nm) were spin-coated from a solution of DTS-based oligomers:PC₇₀BM with various weight ratios in chloroform. Photovoltaic layers within DTS(Oct)₂-(2T-DCV-Me)₂:PC₇₀BM (1:0.8, wt%) were also spin-coated but processed with 50 °C hot solution. In addition, photovoltaic layers within DTS(Oct)₂-(2T-DCV)₂:PC₇₀BM (1:2.5, wt%) were doctor-bladed on top of PEDOT:PSS layer due to worse molecular solubility. After that, the blend films were processed with SVA treatments by using a small petri dish with cover. Finally, a calcium/aluminium top electrode of 15/100 nm thickness was evaporated. In addition, ZnO thin films bladed on top of the active layer were obtained from ZnO precursor solution (nanoparticle suspensions, provided by NanoGrade, Lot#5039). The optimized thickness

of the ZnO layer is approximately 25nm. PDINO layer (ca. 5 nm) was also doctor-bladed on top of the active layer in ambient air from 0.1% PDINO (w/v) solutions in methanol without any other post-processing. The typical active area of the investigated devices was 10.4 mm².

The current-voltage characteristics of OSCs were measured under AM 1.5G irradiation on an OriolSol1A Solar simulator (100 mW cm⁻²). The light source was calibrated by using a silicon reference cell. The device performances mentioned in this paper are corrected to the EQE of the particular device. The EQE was detected with Cary 500 Scan UV-vis-NIR Spectrophotometer under mono-chromatic illumination, which was calibrated with a mono-crystalline silicon diode. In order to study the intensity dependence of J_{sc} and V_{oc} and the intensity dependence of photocurrent, the light intensity was modulated with a series of neutral color density filters, allowing users to change the light intensity from 100 to 1 mW cm⁻². The light intensity transmitted through the filter was independently measured via a power meter.

Single carrier devices were fabricated and the dark current-voltage characteristics measured and analyzed in the space charge limited (SCL) regime following the references. The structure of hole only devices was Glass/ITO/PEDOT:PSS/Active layer/MoO₃ (15 nm)/Ag (100 nm). For the electron only devices, the structure was Glass/ITO/ZnO/Active layer/Ca (15 nm)/Ag (80 nm), where both Ca and Ag were evaporated. The reported mobility data are average values over the twelve devices of each sample.

In photo-CELIV measurements, the devices were illuminated with a 405 nm laser-diode. Current transients were recorded across the internal 50 Ω resistor of our oscilloscope. Here we used a fast electrical switch to isolate the cell during the laser pulse and the delay time, in order to prevent charge extraction or sweep out. After the variable delay time, the switch connected the solar cell to a Function Generator, which applied a linear extraction ramp. The ramp was 60μs long and 2.0 V high, and it started with an offset matching the V_{oc} of the cell for each delay time.

2. Results and discussion

2.1 ^1H and ^{13}C NMR spectra of the DTS-based oligomers

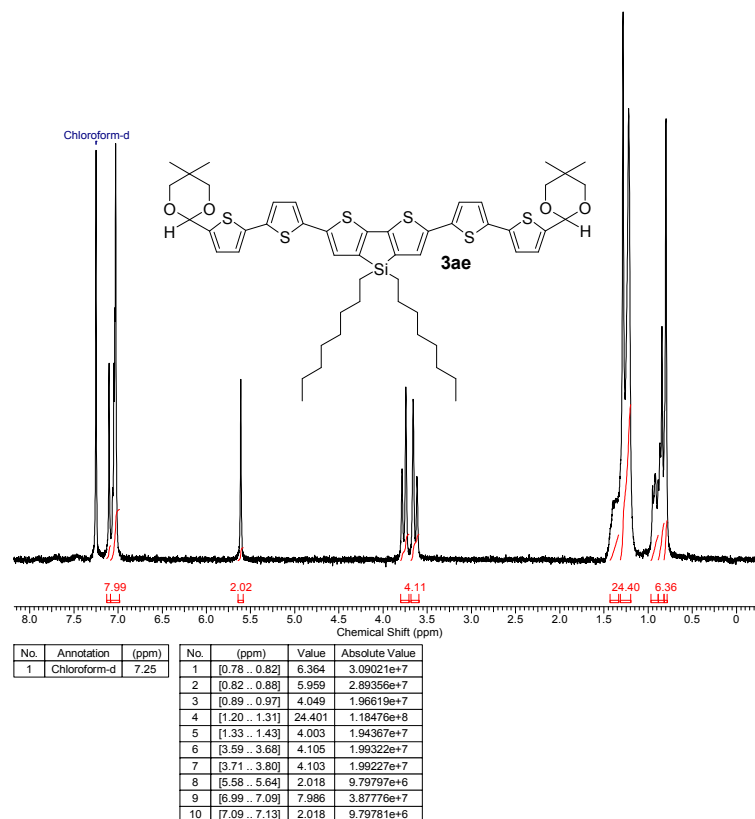


Figure S1. ^1H NMR spectrum of compound 3ae in CDCl_3

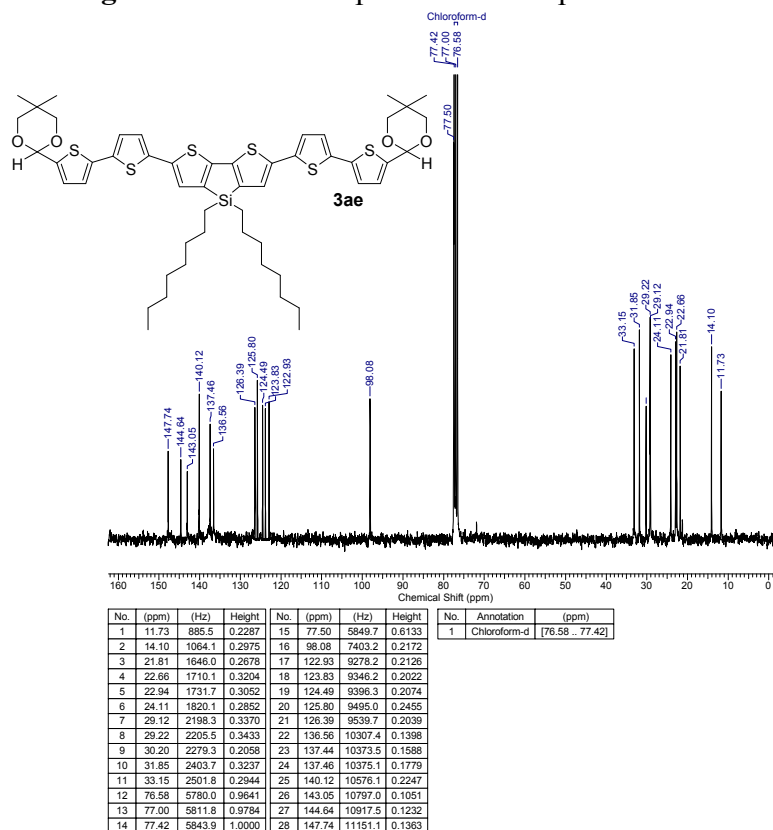


Figure S2. ^{13}C NMR spectrum of compound 3ae in CDCl_3

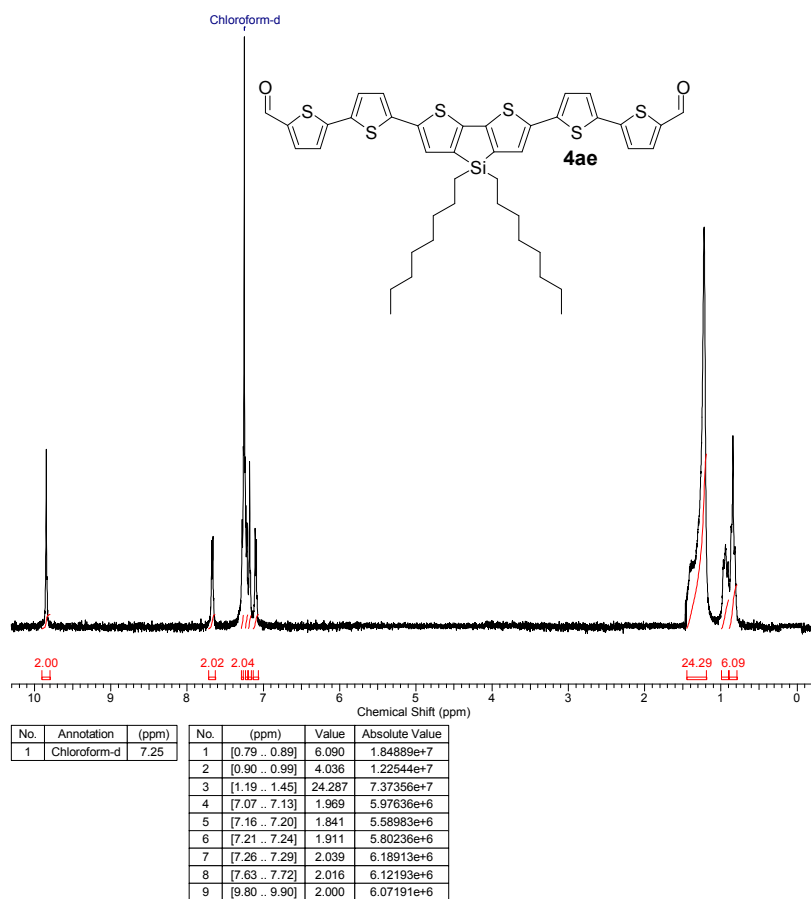


Figure S3. ^1H NMR spectrum of compound **4ae** in CDCl_3

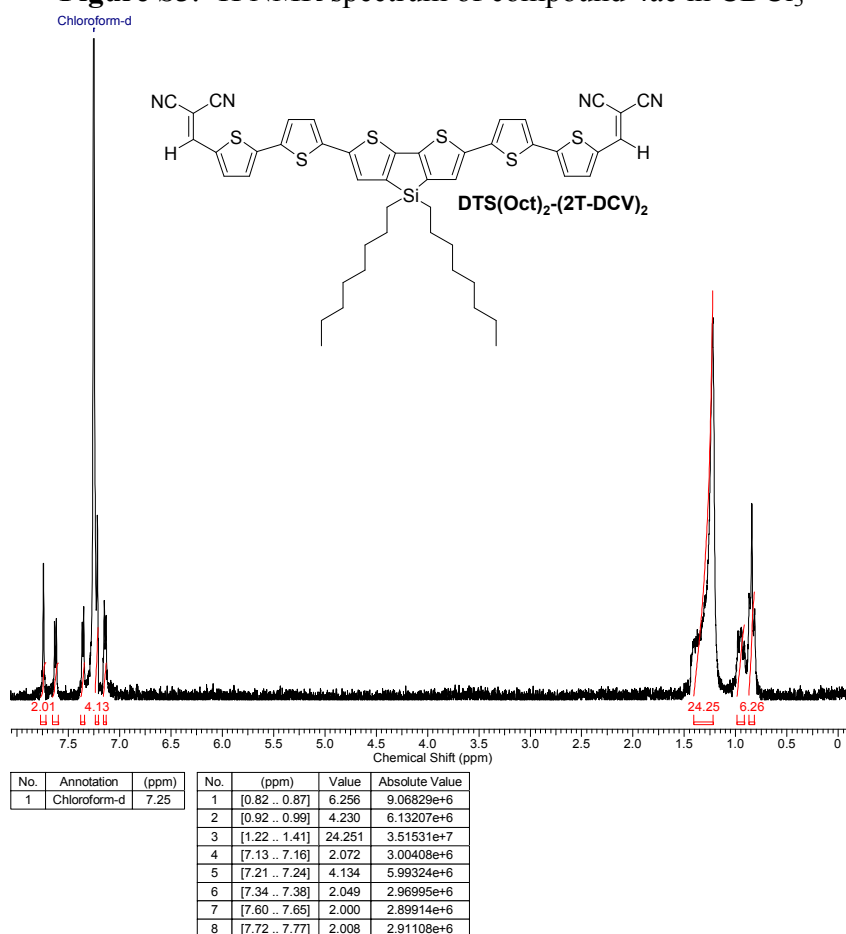


Figure S4. ^1H NMR spectrum of **DTS(Oct)₂-(2T-DCV)₂** in CDCl_3

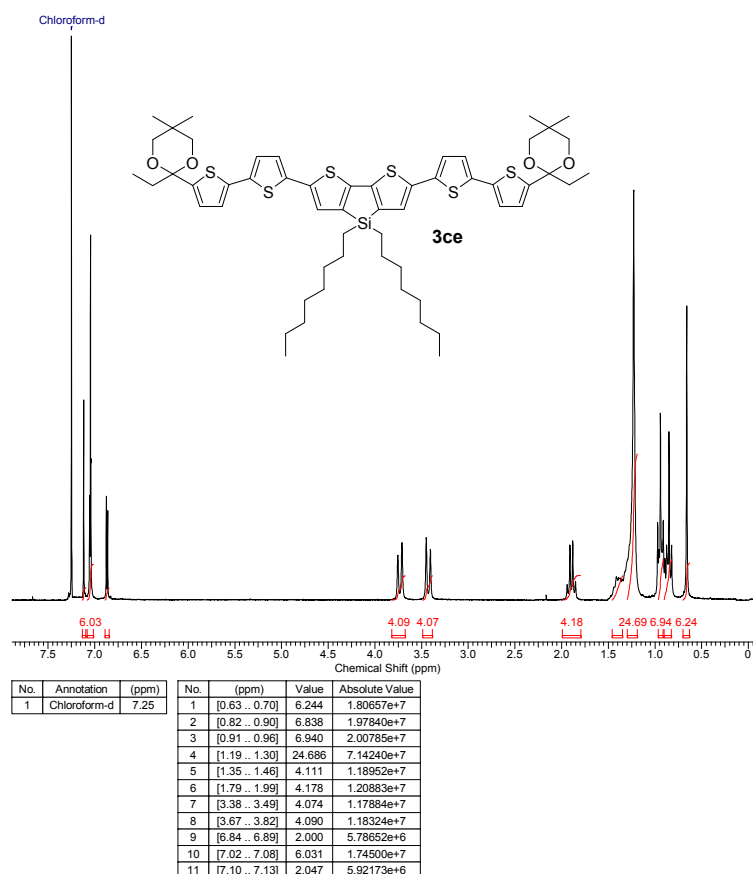


Figure S5. ^1H NMR spectrum of compound 3ce in CDCl_3

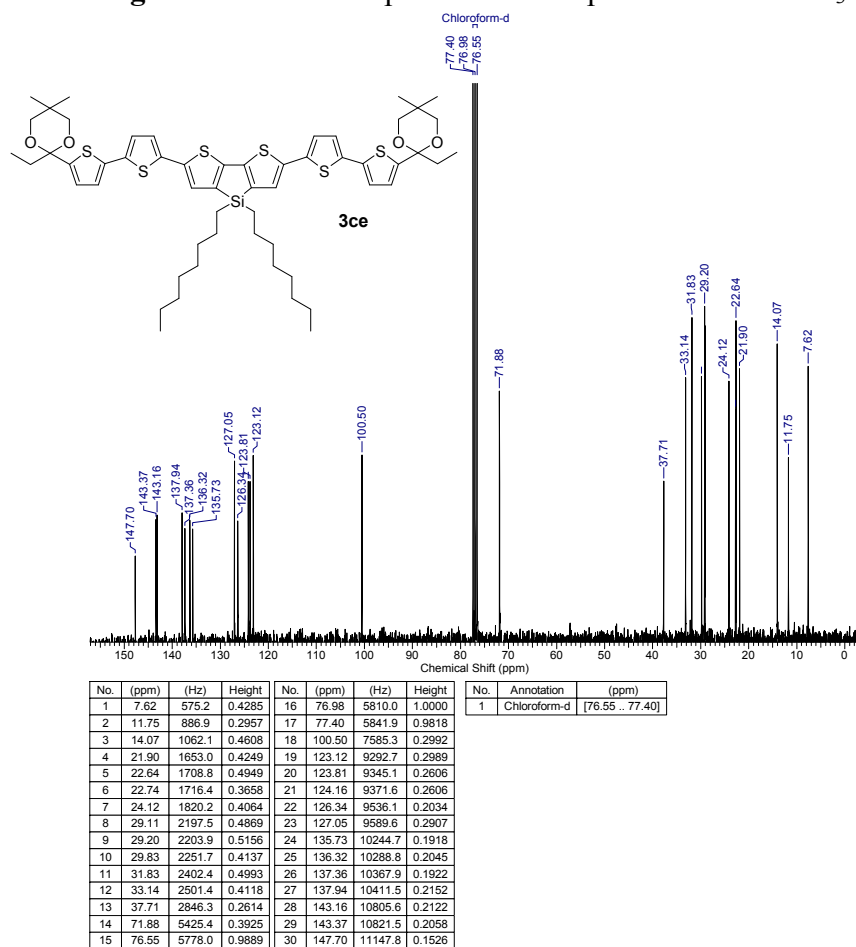


Figure S6. ^{13}C NMR spectrum of compound 3ce in CDCl_3

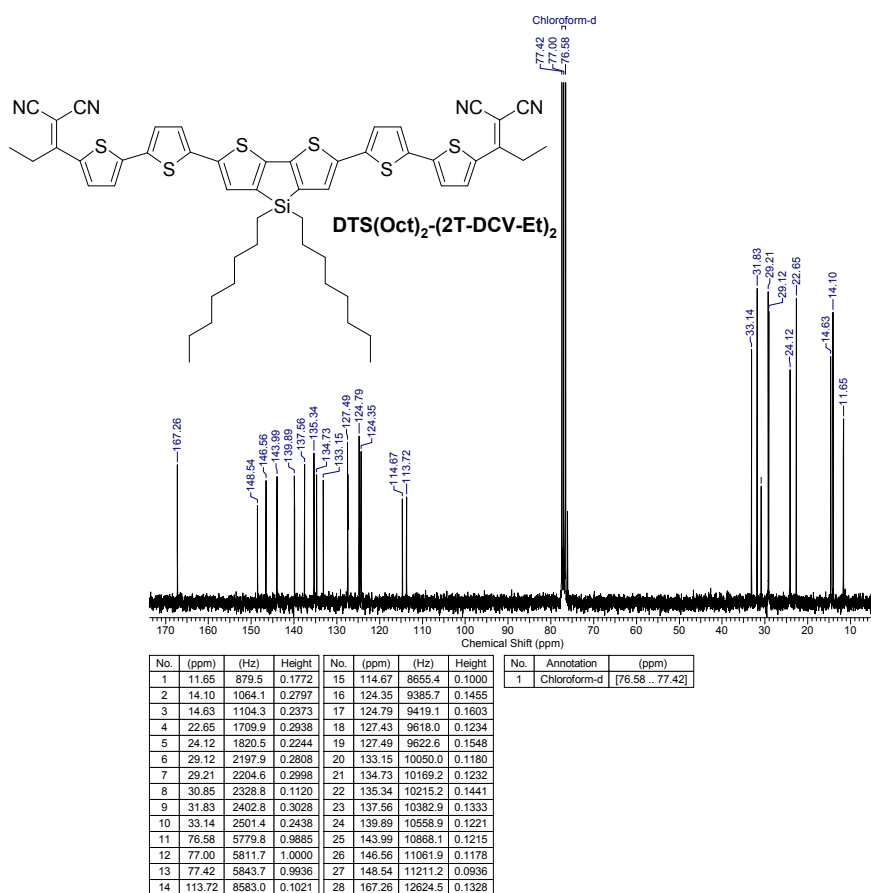


Figure S9. ¹³C NMR spectrum of compound DTS(Oct)₂-(2T-DCV-Et)₂ in CDCl₃

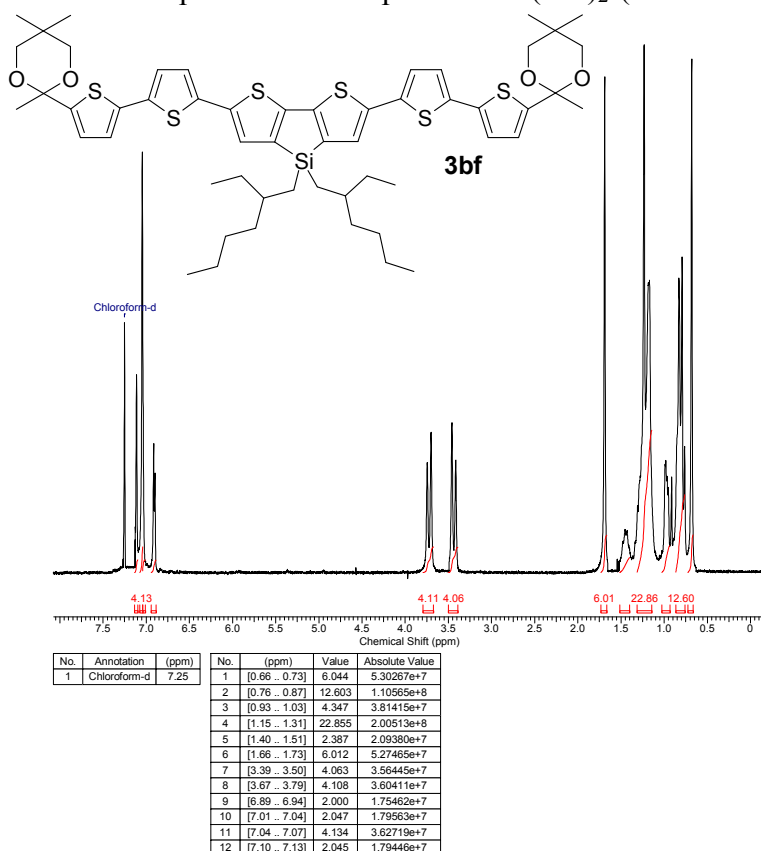


Figure S10. ¹H NMR spectrum of compound 3bf in CDCl₃

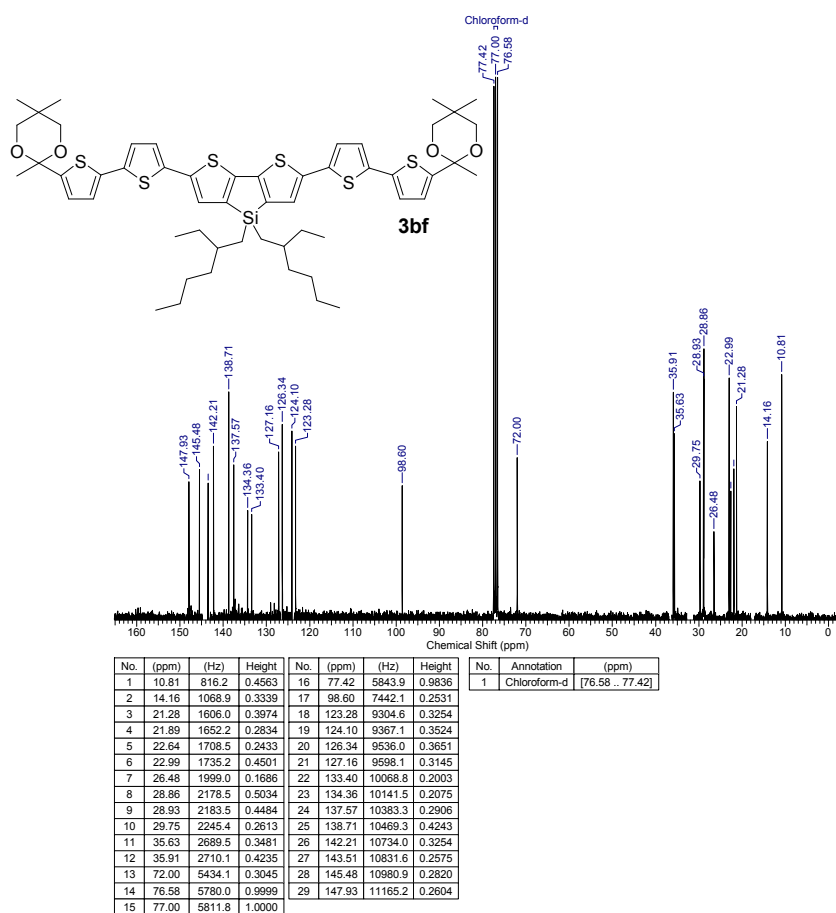


Figure S11. ^{13}C NMR spectrum of compound 3bf in CDCl_3

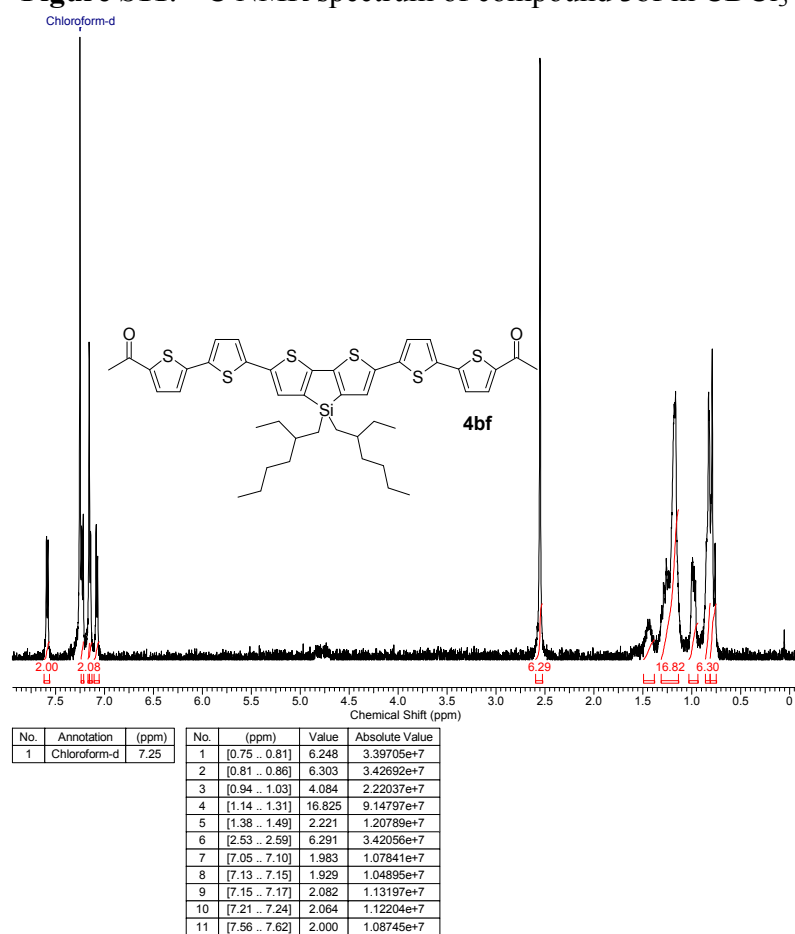


Figure S12. ^1H NMR spectrum of compound 4bf in CDCl_3

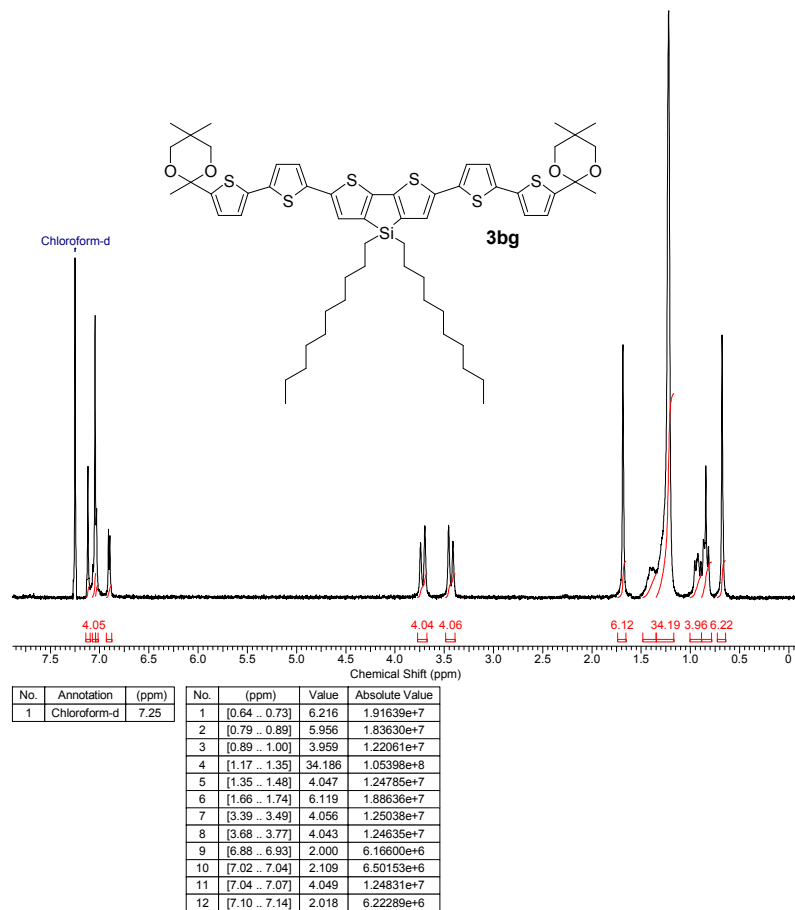


Figure S15. ¹H NMR spectrum of compound 3bg in CDCl₃

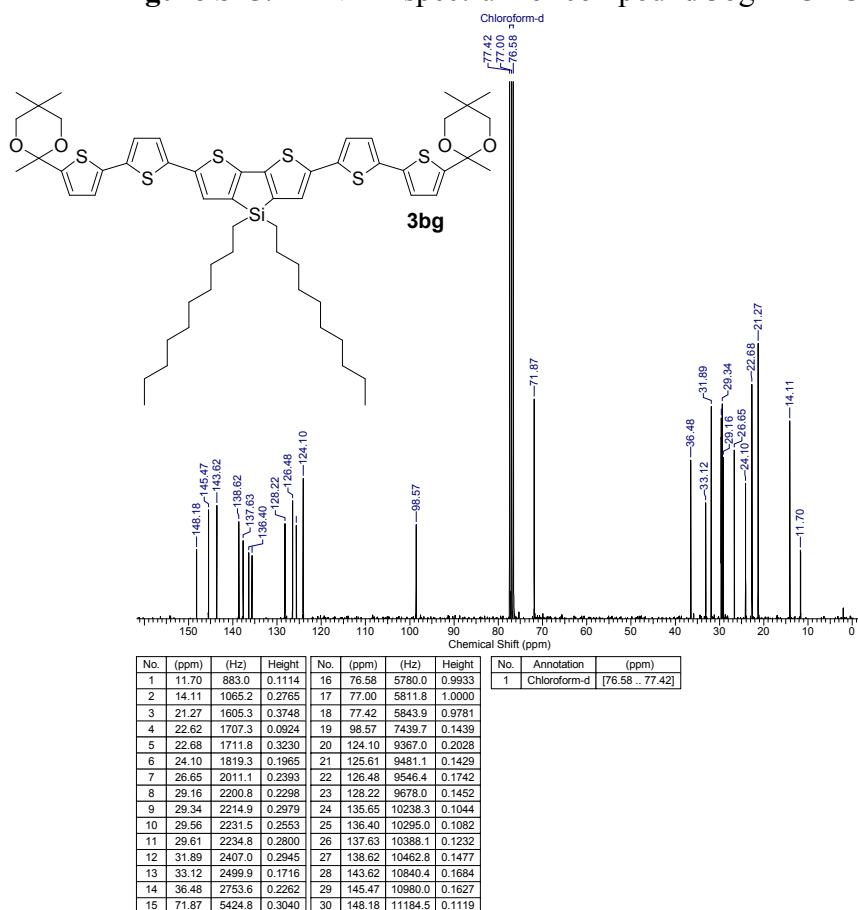


Figure S16. ¹³C NMR spectrum of compound 3bg in CDCl₃

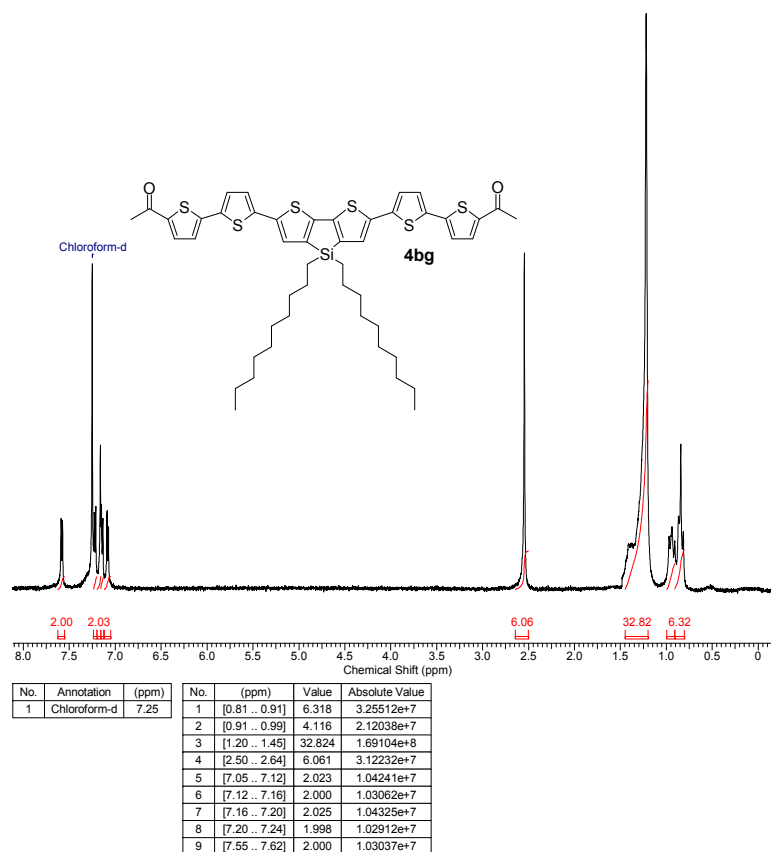


Figure S17. ^1H NMR spectrum of compound 4bg in CDCl_3

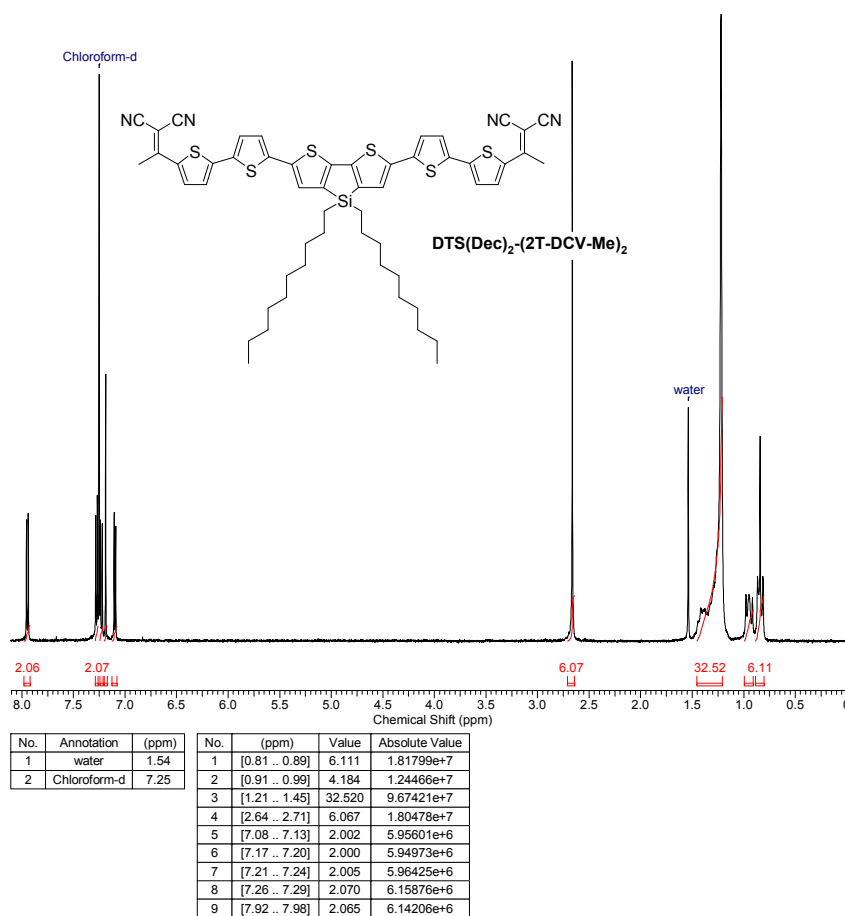


Figure S18. ^1H NMR spectrum of $\text{DTS}(\text{Dec})_2-(2\text{T-DCV-Me})_2$ in CDCl_3

2.2 Thermal properties of the DTS-based oligomers

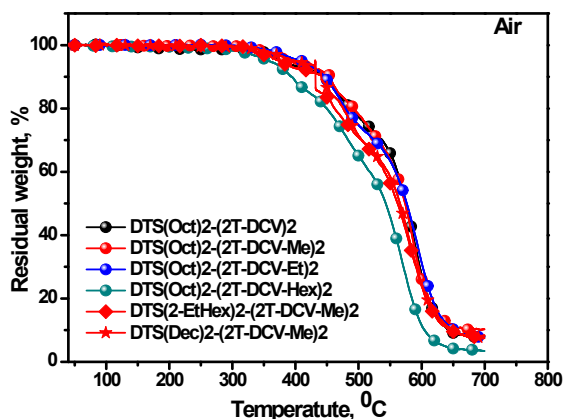


Figure S20. TGA curves of DTS-based oligomers in air.

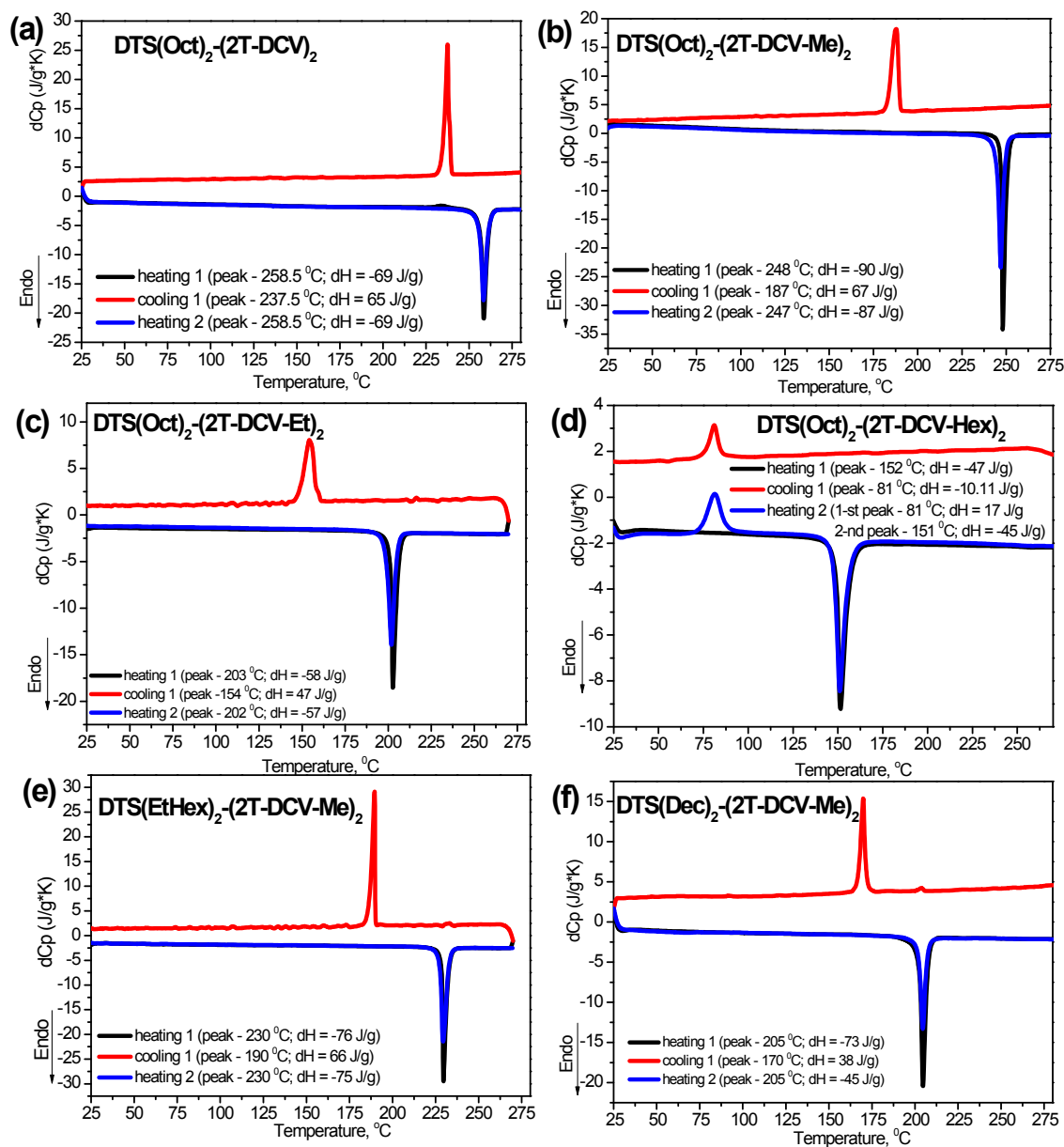


Figure S21. Differential scanning calorimetry (DSC) scans of (a) $\text{DTS}(\text{Oct})_2-(2\text{T-DCV})_2$; (b) $\text{DTS}(\text{Oct})_2-(2\text{T-DCV-Me})_2$; (c) $\text{DTS}(\text{Oct})_2-(2\text{T-DCV-Et})_2$; (d) $\text{DTS}(\text{Oct})_2-(2\text{T-DCV-Hex})_2$; (e) $\text{DTS}(\text{EtHex})_2-(2\text{T-DCV-Me})_2$; (f) $\text{DTS}(\text{Dec})_2-(2\text{T-DCV-Me})_2$. For the sake of simplicity, curves are shifted along heat flow axis.

2.3 Optical and electrochemical properties of the DTS-based oligomers

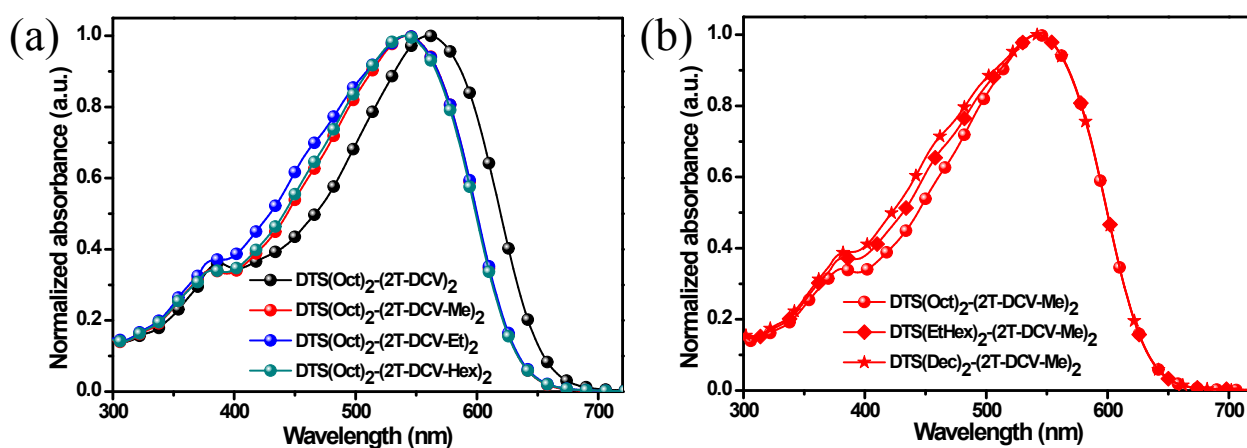


Figure S22. UV-vis absorption spectra of the DTS-based oligomers (a) with alkyl terminal chains and (b) with alkyl chains on donor unit in chloroform solution.

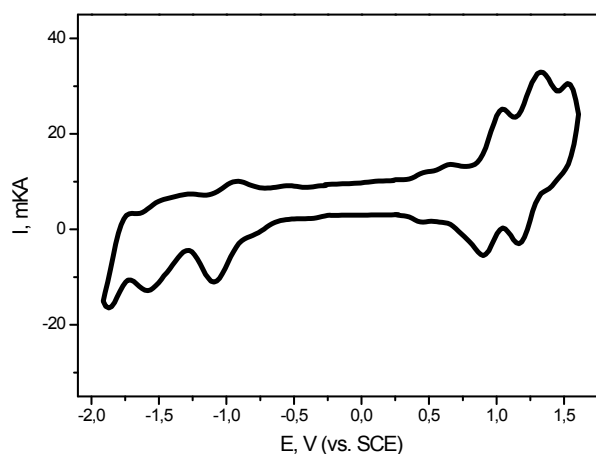


Figure S23. Electrochemical oxidation (a) and reduction (b) curves of DTS(Oct)₂-(2T-DCV-Hex)₂ in ODCB-acetonitrile solutions.

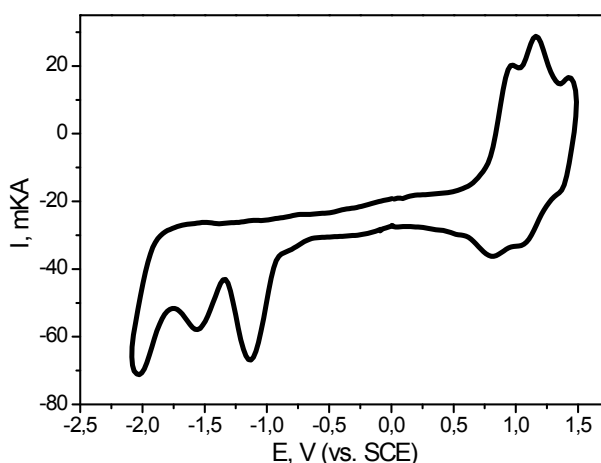


Figure S24. Cyclic voltammograms of DTS(Oct)₂-(2T-DCV-Hex)₂ in film as the example to illustrate the difference of oxidation and reduction as compared to the CVs of DTS-based containing oligomers in ODCB-acetonitrile solution.

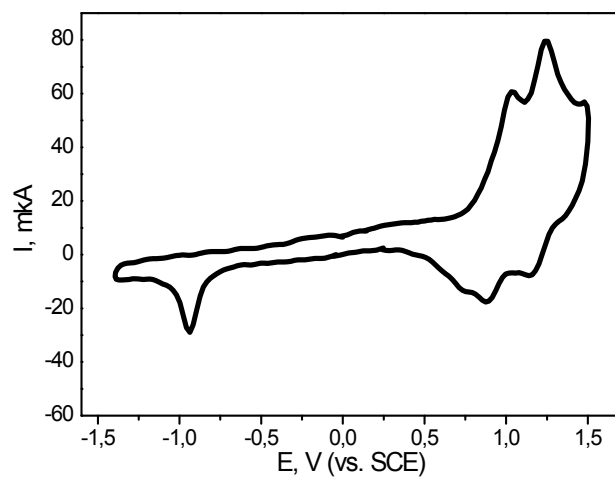


Figure S25. Cyclic voltammograms of $\text{DTS}(\text{Oct})_2\text{-(2T-DCV)}_2$ in film.

2.4 Photovoltaic properties of the DTS-based oligomers

Figure S26. (a) conventional architectures of oligomer:PC₇₀BM BHJ solar cells used in this study; schematic representation of the band energy diagrams for the conventional configurations of SMOSCs based on (b) the metal cathodes, (c) ZnO/Al cathode and (d) PDINO/Ag cathode.

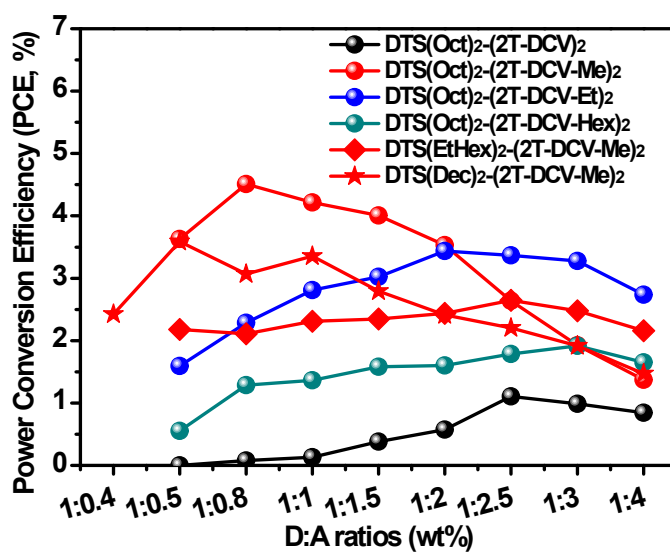


Figure S27. Photovoltaic performance of the DTS-based oligomers in devices based on various D:A weight ratios.

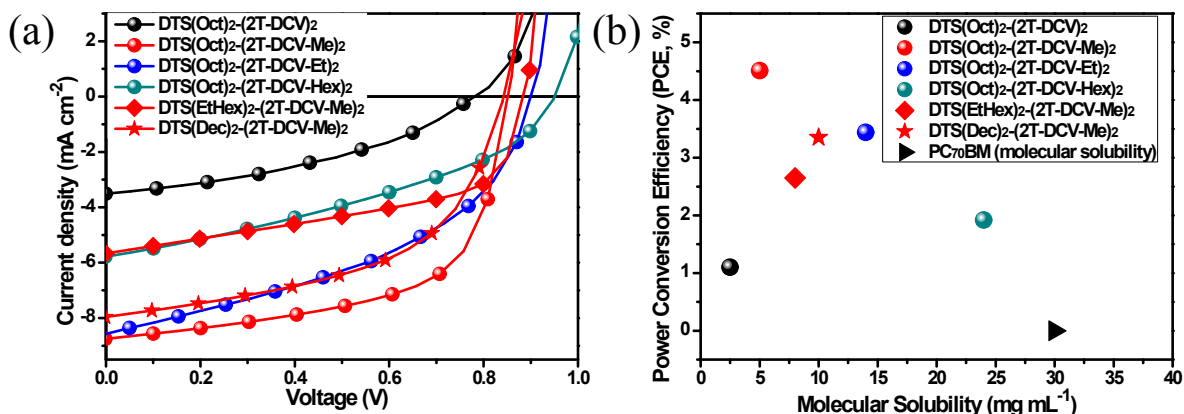


Figure S28. (a) J - V characteristics of DTS-based oligomers based solar cells with optimized D:A ratios measured under 100 mW cm⁻² AM 1.5 G illumination; (b) Power conversion efficiencies (PCEs) of DTS-based oligomers based solar cells with optimized D:A ratios verse as a function of molecular solubility. The inset also shows the solubility of PC₇₀BM measured under the same conditions.

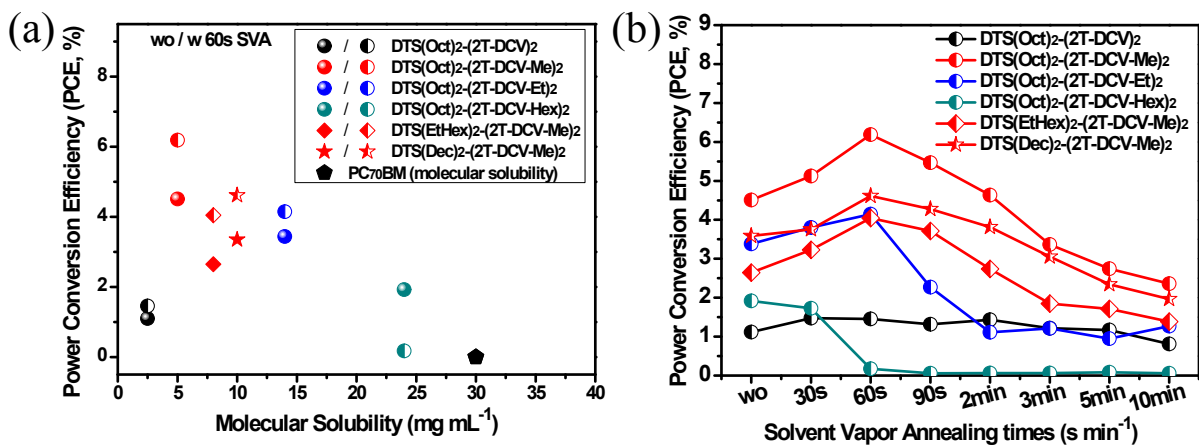


Figure S29. (a) the PCEs of devices without and with 60s SVA treatments verse as a function of molecular solubility; (b) the PCEs of devices with SVA process verse as a function of process time.

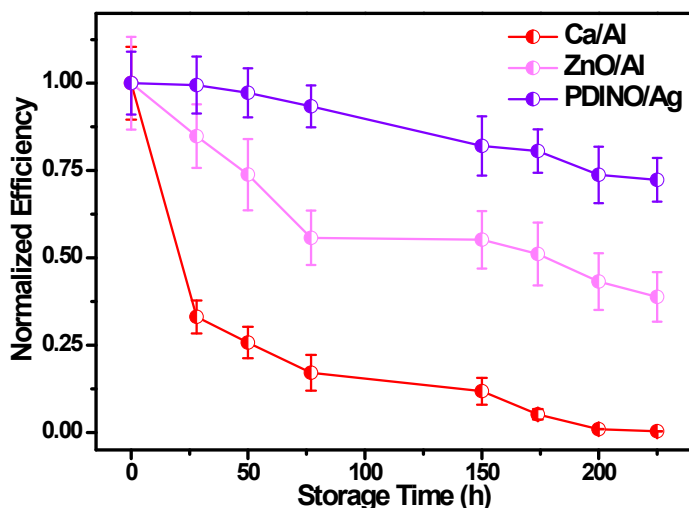


Figure S30. Normalized cell efficiency plotted as a function of storage time for solar cells with Ca/Al, ZnO/Al, and PDINO/Ag cathodes stored in air. Measurements were made on six devices of each type without any encapsulation, and the error bars represent plus or minus 1 standard deviation from the mean.

2.5 Morphology Characterizations and Investigations

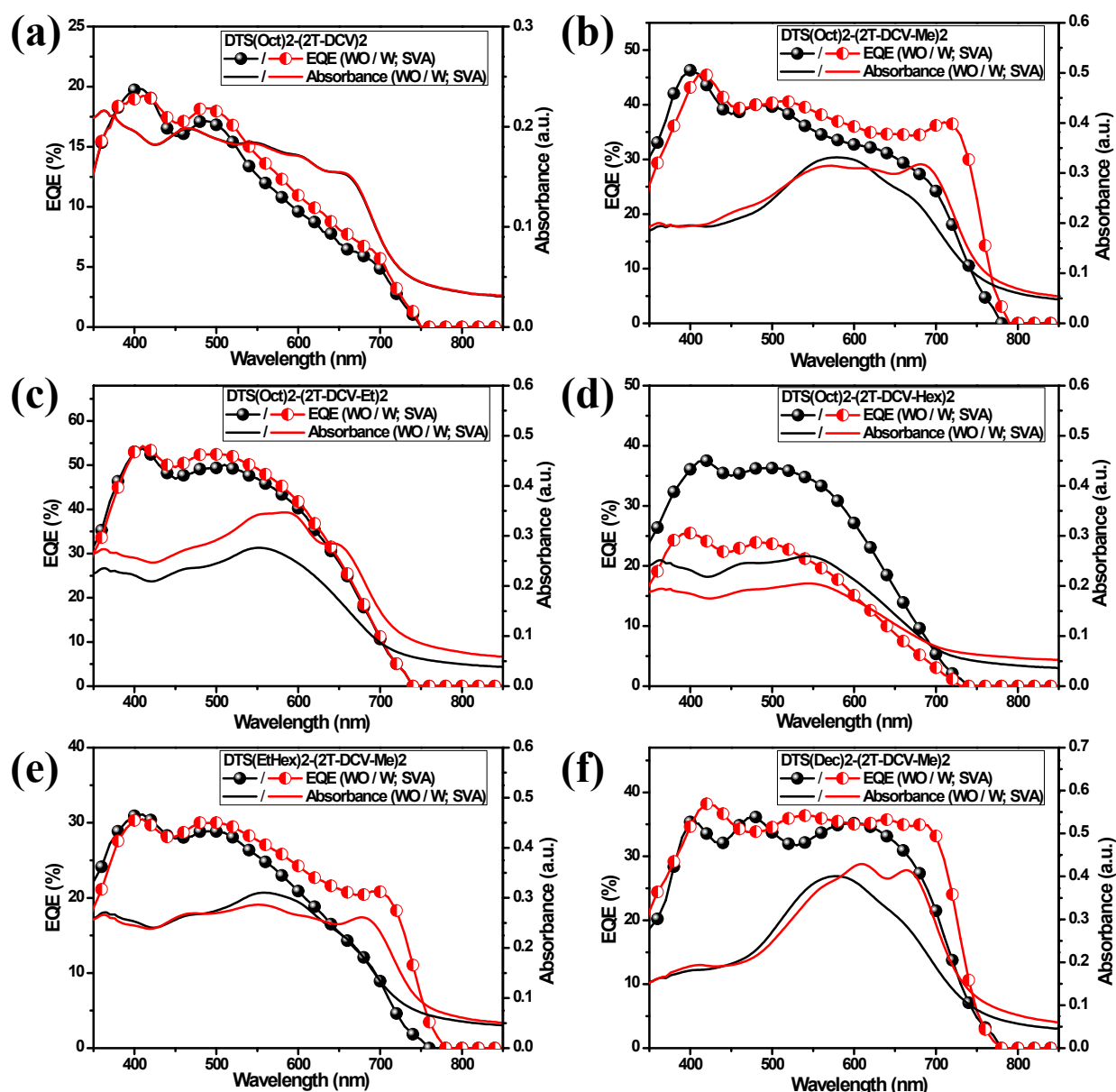


Figure S31. EQE spectra of the devices based on various DTS-based oligomer systems, including: (a) $\text{DTS}(\text{Oct})_2\text{-(2T-DCV)}_2$, (b) $\text{DTS}(\text{Oct})_2\text{-(2T-DCV-Me)}_2$, (c) $\text{DTS}(\text{Oct})_2\text{-(2T-DCV-Et)}_2$, (d) $\text{DTS}(\text{Oct})_2\text{-(2T-DCV-Hex)}_2$, (e) $\text{DTS}(\text{EtHex})_2\text{-(2T-DCV-Me)}_2$, and (f) $\text{DTS}(\text{Dec})_2\text{-(2T-DCV-Me)}_2$; and absorption spectra of these related blend films on glass substrates (pre-coated with 40 nm thick PEDOT:PSS films).

Optical absorption spectra of these DTS-based oligomers blend films (pre-coated with 40 nm thick PEDOT:PSS films on glass-substrates) as well as the EQE spectra of these DTS-based oligomers based devices with and without SVA treatments are presented in Figure S31. After SVA treatment, the spectral shape of the absorption from $\text{DTS}(\text{Oct})_2\text{-(2T-DCV)}_2$ film is relatively unchanged (Figure S31a), due to the low molecular solubility. Having been annealed, the blend films of $\text{DTS}(\text{Oct})_2\text{-(2T-DCV-Me)}_2$, $\text{DTS}(\text{Oct})_2\text{-(2T-DCV-Et)}_2$, $\text{DTS}(\text{EtHex})_2\text{-(2T-DCV-Me)}_2$, $\text{DTS}(\text{Dec})_2\text{-(2T-DCV-Me)}_2$

(2T-DCV-Me)₂ show the enhanced absorption spectra and somewhat obvious shoulder peaks in the long wavelength similar to the absorption spectra of pristine oligomers. These observations suggest that SVA promotes some enhanced crystallinity of the DTS oligomers leading to differentiation of their absorption spectra (Figure S31b, c, e and f). However, the DTS(Oct)₂-(2T-DCV-Hex)₂ with a high solubility in contrast shows a worse absorption spectra of the annealed film as compared to that of the film without SVA treatment (see Figure S31d). In addition, apart from the J_{sc} of various devices mentioned above, the EQE spectra are also in agreement with the absorption spectra of blend films. This phenomenon may be attributed to the similar solubility between DTS(Oct)₂-(2T-DCV-Hex)₂ and PC₇₀BM and thus result in the inefficient phase separations in blends. Thus the SVA treatment further leads to the worse inhomogeneous miscibility in DTS(Oct)₂-(2T-DCV-Hex)₂ blends. The higher EQE values of annealed devices based on DTS(Oct)₂-(2T-DCV-Me)₂, DTS(Oct)₂-(2T-DCV-Et)₂, DTS(EtHex)₂-(2T-DCV-Me)₂, DTS(Dec)₂-(2T-DCV-Me)₂ in the donor absorption region prove that SVA treatments effectively facilitate molecular packing and improve blend morphologies, and thus successfully increase the related photovoltaic properties. In short, the observed differences in absorption spectra and EQE data as well as the techniques taken together suggest a number of different phases depending on the molecular isomer or homologue type, molecular solubility and morphological control method.

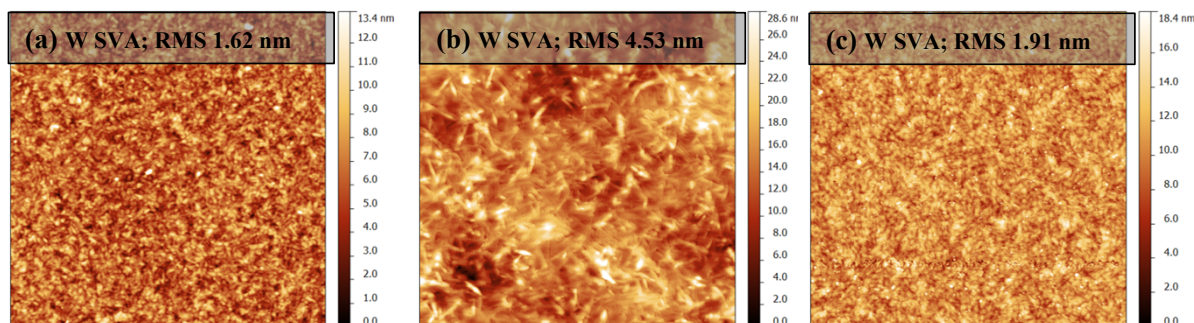


Figure S32. Surface topographic AFM images (size: $5 \times 5 \mu\text{m}^2$) of DTS(Oct)₂-(2T-DCV-Me)₂ blend film with 60s (a) and 5 min (b) SVA process, (c) after deposition of thin PDINO layer on the DTS(Oct)₂-(2T-DCV-Me)₂ blend film with 60s SVA process.

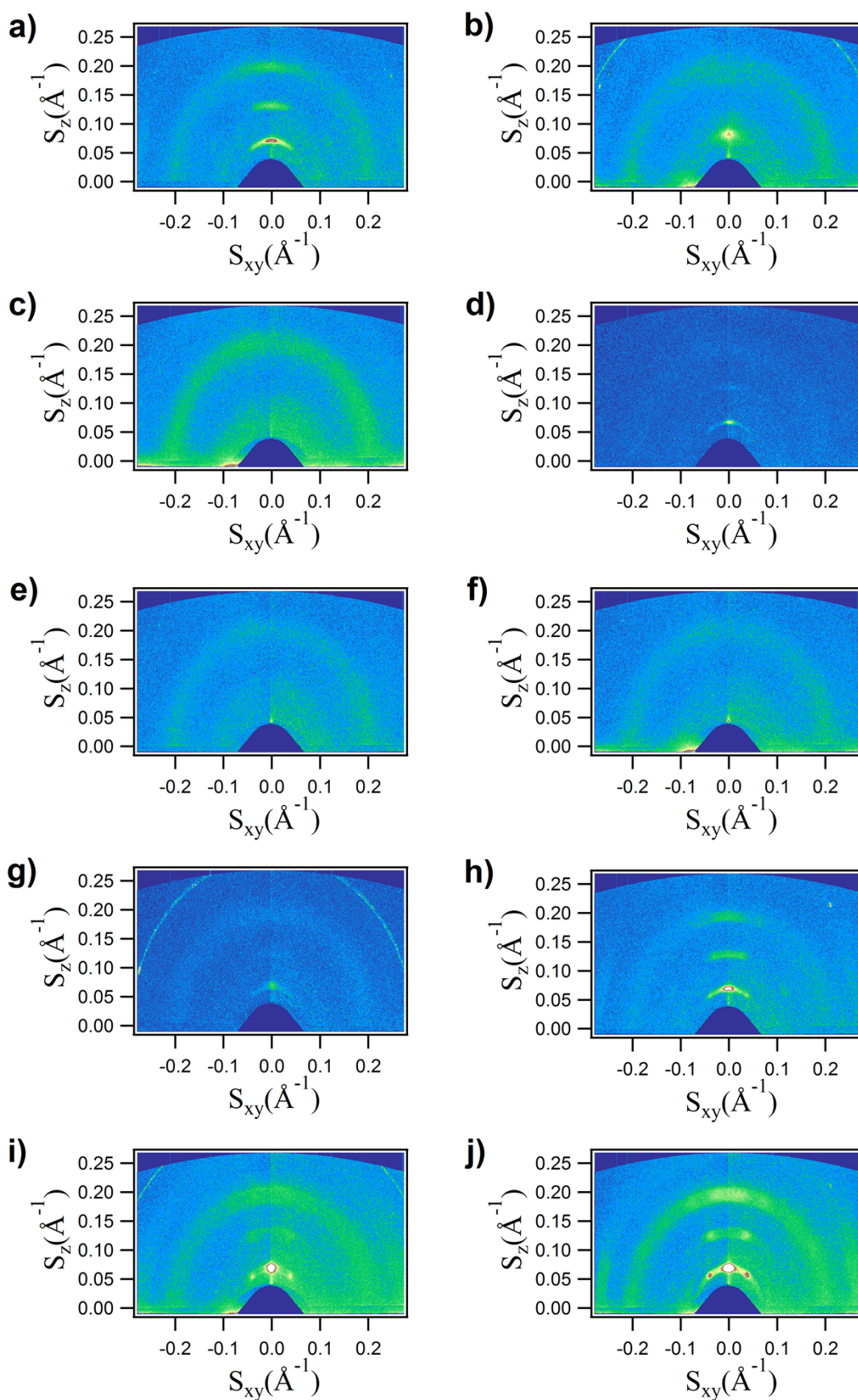


Figure S33. 2D GIWAXS patterns of the blended films of PC70BM and (a, b) DTS(Oct)₂-2T-DCV)₂:PC₇₀BM, (c, d) DTS(Oct)₂-2T-DCV-Et)₂, (e, f) DTS(Oct)₂-2T-DCV-Hex)₂, (g, h) DTS(EtHex)₂-2T-DCV-Me)₂, (i, j) DTS(Dec)₂-2T-DCV-Me)₂, where (a, c, e, g, i) before and (b, d, f, h, j) after SVA treatments

Table S1. Experimental and calculated d-spacings for the monoclinic lattice of DTS(Dec)₂-(2T-DCV-Me)₂:PC₇₀BM.

h	k	L	d _{exp} , Å	d _{calc} , Å
0	0	2	14.52	14.50
1	0	1	14.56	14.56
1	1	1	7.71	7.66
1	0	5	5.1	5.15
1	2	-4	3.8	3.9

Table S2. Experimental d-spacings extracted from 2D-diffractograms for samples without (WO) and with (W) SVA treatments.

Sample oligomer:PC ₇₀ BM	SVA	d1	d2*	d3	d4*	d5
DTS(Oct) ₂ -(2T-DCV) ₂ :PC ₇₀ BM	WO	14.13	10.5	7.59	5.03	
DTS(Oct) ₂ -(2T-DCV) ₂ :PC ₇₀ BM	W	12.4	10.3		5.08	
DTS(Oct) ₂ -(2T-DCV-Me) ₂ :PC ₇₀ BM	WO	13.86	10.4	7.41	5.00	
DTS(Oct) ₂ -(2T-DCV-Me) ₂ :PC ₇₀ BM	W	14.1	10.3	7.51	5.03	3.78
DTS(Oct) ₂ -(2T-DCV-Et) ₂ :PC ₇₀ BM	WO	15.79	10.0		4.93	
DTS(Oct) ₂ -(2T-DCV-Et) ₂ :PC ₇₀ BM	W	15.05	10.1	7.92	5.1	
DTS(Oct) ₂ -(2T-DCV-Hex) ₂ :PC ₇₀ BM	WO	13.7	10.5	5.12	5.04	
DTS(Oct) ₂ -(2T-DCV-Hex) ₂ :PC ₇₀ BM	W	16.34	10.5	4.97	5.06	
DTS(EtHex) ₂ -(2T-DCV-Me) ₂ :PC ₇₀ BM	WO	14.65	10.5		5.14	
DTS(EtHex) ₂ -(2T-DCV-Me) ₂ :PC ₇₀ BM	W	14.51	10.4	7.75	5.13	3.76
DTS(Dec) ₂ -(2T-DCV-Me) ₂ :PC ₇₀ BM	WO	14.54	10.5	7.56	5.06	3.7
DTS(Dec) ₂ -(2T-DCV-Me) ₂ :PC ₇₀ BM	W	14.52	10.4	7.71	5.1	3.76

* reflections of a pure PC₇₀BM structure.

The effect of the substrate was addressed using an example of the DTS(Oct)₂-(2T-DCV-Me)₂:PC₇₀BM film (cf. Figure S33, Table S3). One can see that the sample deposited on glass covered with PEDOT:PSS shows a less organized structure before and after annealing compared to the film on silicon. The increase of the radial peak width and a decrease of the intensity is probably related to a higher roughness of the glass surface.

Table S3. Experimental d-spacings for DTS(Oct)₂-(2T-DCV-Me)₂ films deposited on silicon and glass

Sample oligomer:PC ₇₀ BM	substrate	d1	d2	d3	d4	d5
DTS(Oct) ₂ -(2T-DCV-Me) ₂ :PC ₇₀ BM WO	silicon	13.86	10.4	7.41	5	
DTS(Oct) ₂ -(2T-DCV-Me) ₂ :PC ₇₀ BM W	silicon	14.1	10.3	7.51	5.03	3.78
DTS(Oct) ₂ -(2T-DCV-Me) ₂ :PC ₇₀ BM WO	glass/PEDOT:PSS	14.03	10.3	7.18	5.02	
DTS(Oct) ₂ -(2T-DCV-Me) ₂ :PC ₇₀ BM W	glass/PEDOT:PSS	14	10.2	7.55	4.9	

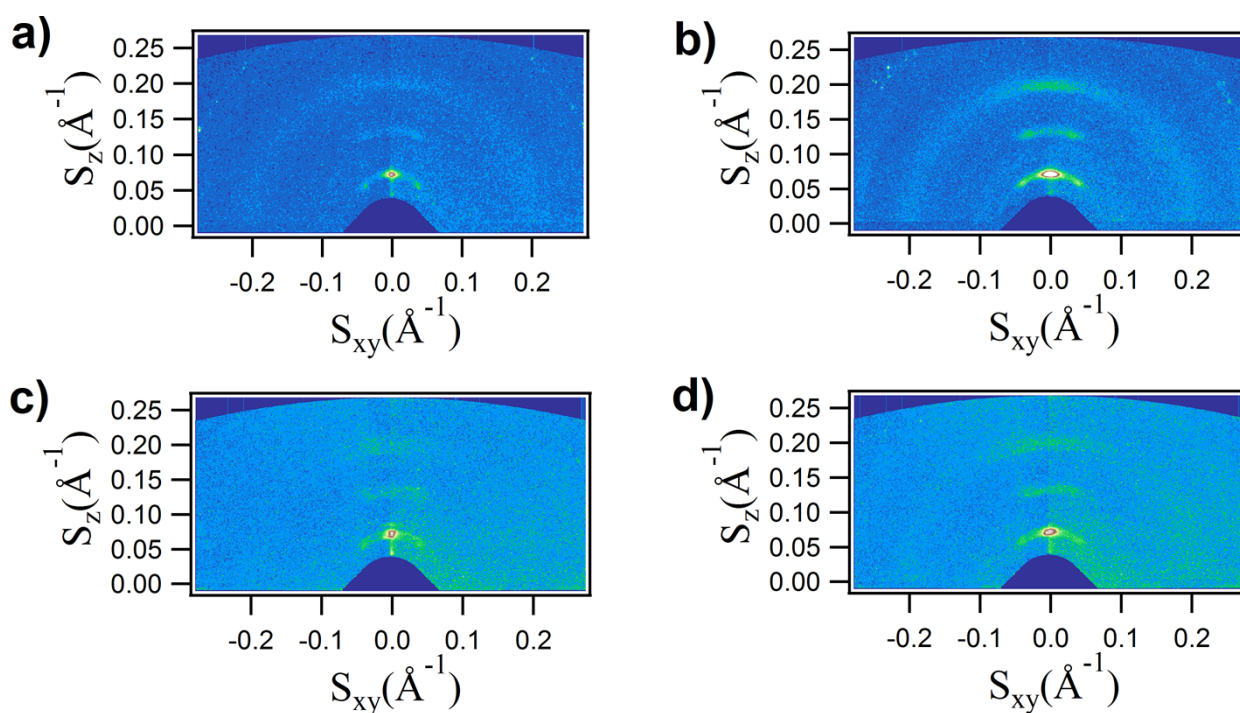


Figure S34. 2D GIWAXS patterns of DTS(Oct)₂-(2T-DCV-Me)₂:PC₇₀BM on (a,b) silicon substrate and (c,d) glass covered with PEDOT:PSS before (a,c) and after (b,d) SVA

2.6 Charge transport properties and recombination dynamics

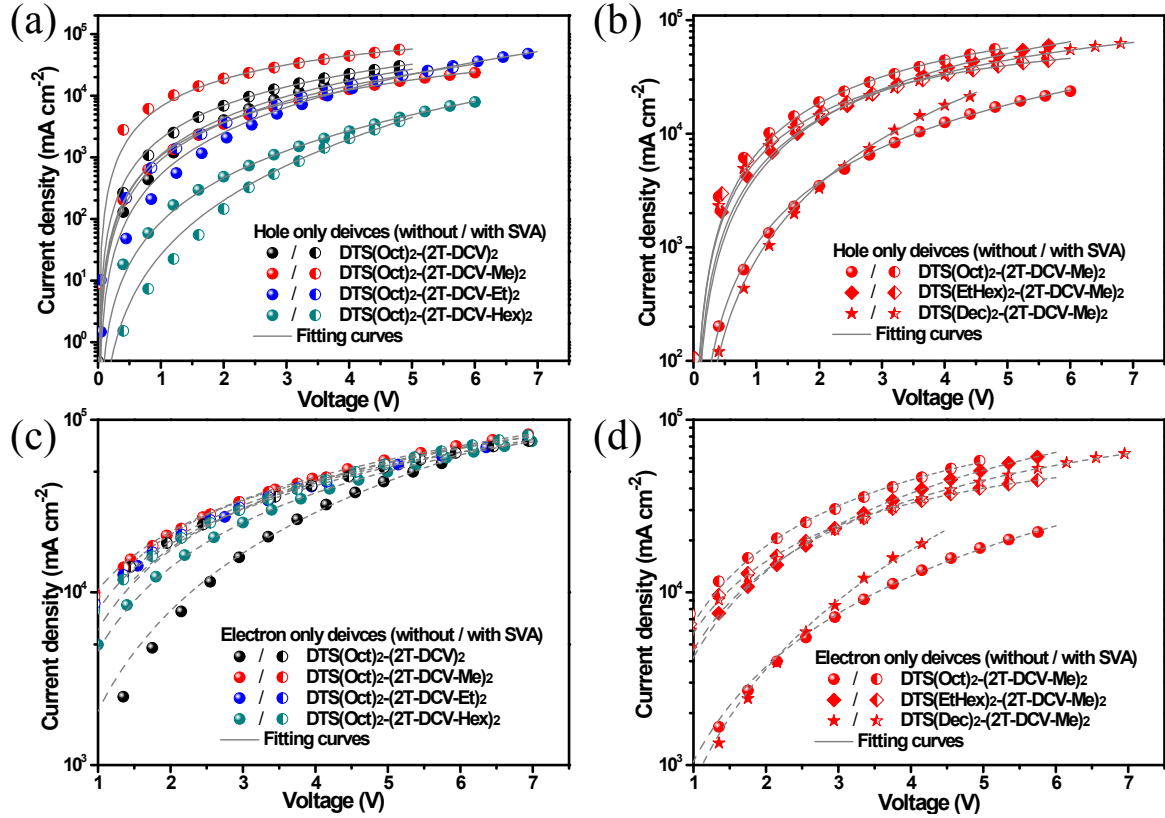


Figure S35. The dark J - V characteristics of (a, c) DTS-based oligomers with various alkyl terminal chains and (b, d) DTS-based oligomers with various alkyl chains in donor unit based hole-only devices and electron-only devices, respectively. The solid lines represent the best fitting using the SCLC model.

Table S4. Summary of the fitting data for hole-only and electron-only devices based on Mott-Gurney law.

Semiconductor layers	SVA processing (60s)	Thickness (nm)	Hole mobility ^{a,b} ($\text{cm}^2\text{V}^{-1}\text{s}^{-1}$)	Thickness (nm)	Electron mobility ^{a,c} ($\text{cm}^2\text{V}^{-1}\text{s}^{-1}$)
DTS(Oct) ₂ -(2T-DCV) ₂ : PC ₇₀ BM (1:2.5, wt%)	WO W	82 80	1.11×10^{-4} 2.12×10^{-4}	65 72	2.01×10^{-4} 1.02×10^{-3}
DTS(Oct) ₂ -(2T-DCV-Me) ₂ : PC ₇₀ BM (1:0.8, wt%)	WO W	90 95	1.07×10^{-4} 1.01×10^{-3}	75 73	1.17×10^{-3} 1.95×10^{-3}
DTS(Oct) ₂ -(2T-DCV-Et) ₂ : PC ₇₀ BM (1:2, wt%)	WO W	87 92	2.64×10^{-5} 6.68×10^{-5}	78 82	9.83×10^{-4} 1.66×10^{-3}
DTS(Oct) ₂ -(2T-DCV-Hex) ₂ : PC ₇₀ BM (1:3, wt%)	WO W	85 83	3.26×10^{-6} 4.45×10^{-7}	77 71	6.22×10^{-4} 8.44×10^{-4}
DTS(EtHex) ₂ -(2T-DCV-Me) ₂ : PC ₇₀ BM (1:2.5, wt%)	WO W	96 99	1.34×10^{-4} 5.30×10^{-4}	84 85	4.75×10^{-4} 7.32×10^{-4}
DTS(Dec) ₂ -(2T-DCV-Me) ₂ : PC ₇₀ BM (1:0.5, wt%)	WO W	86 85	4.21×10^{-5} 6.33×10^{-4}	79 73	7.43×10^{-4} 1.14×10^{-3}

^aan average value based on twelve devices with the same thickness; ^bthe structure of hole-only device is ITO/PEDOT/Semiconductor/MoO₃/Ag; ^cthe structure of electron-only device is ITO/ZnO/Semiconductor/Ca/Ag.

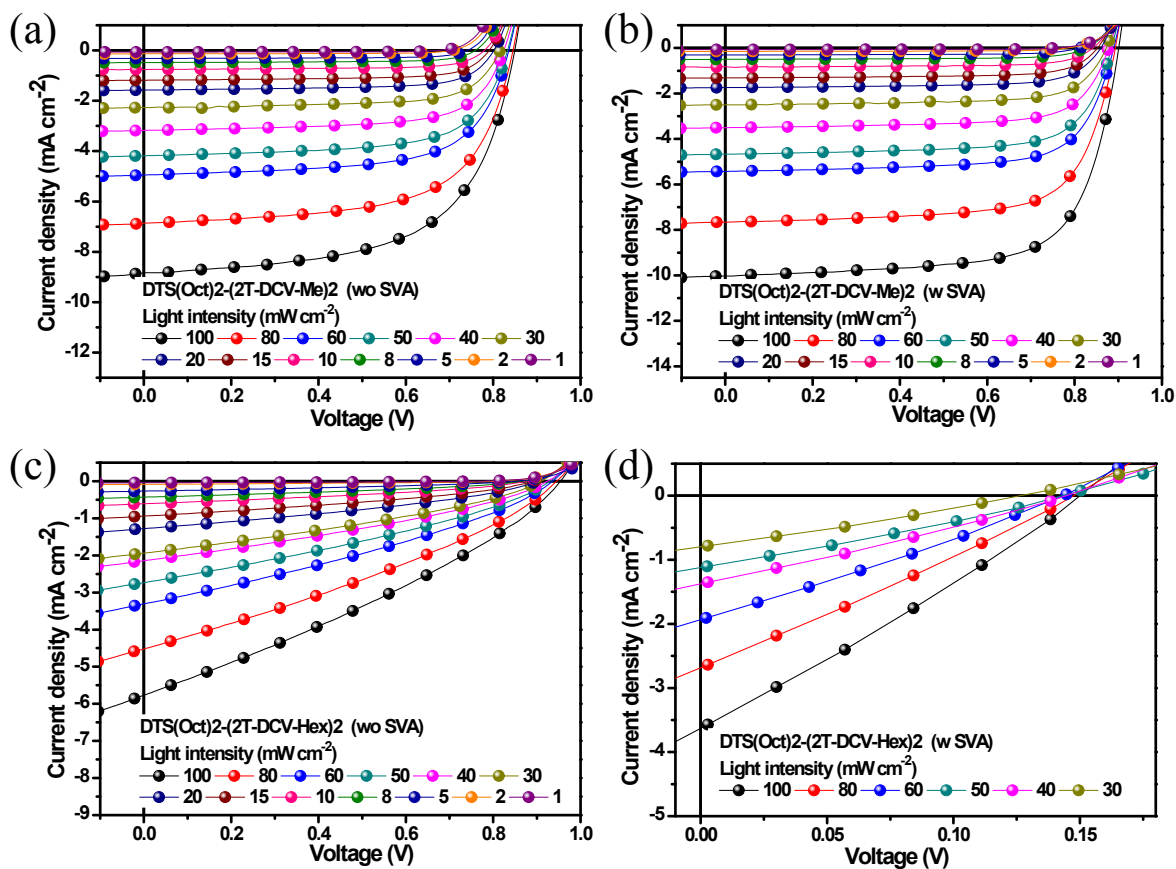


Figure S36. J - V characteristics of DTS(Oct)₂-(2T-DCV-Me)₂:PC₇₀BM devices (a) without and (b) with SVA treatments as well as DTS(Oct)₂-(2T-DCV-Hex)₂:PC₇₀BM devices (c) without and (d) with SVA treatments under various light intensities ranging from 100 mW cm^{-2} to 1 mW cm^{-2} . Neutral density filters were used to control the incident light intensity, which was varied from 1 to 100 mW cm^{-2} .

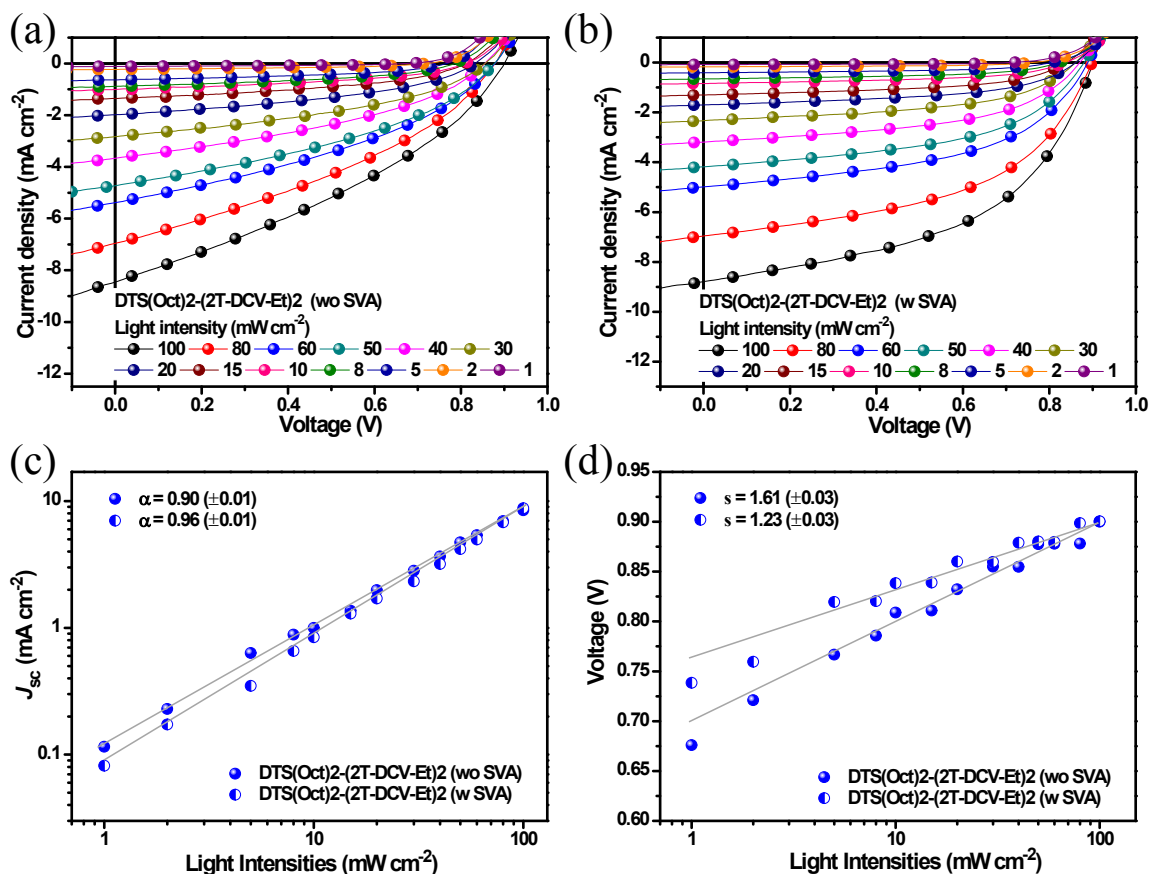


Figure S37. J - V characteristics of DTS(Oct)₂-(2T-DCV-Et)₂:PC₇₀BM devices (a) without and (b) with SVA treatments under various light intensities ranging from 100 mW cm⁻² to 1 mW cm⁻². The measured (c) J_{sc} and (d) V_{oc} of DTS(Oct)₂-(2T-DCV-Et)₂:PC₇₀BM devices with and without SVA treatments as a function of illumination intensity, together with linear fits to the relative data (solid lines).

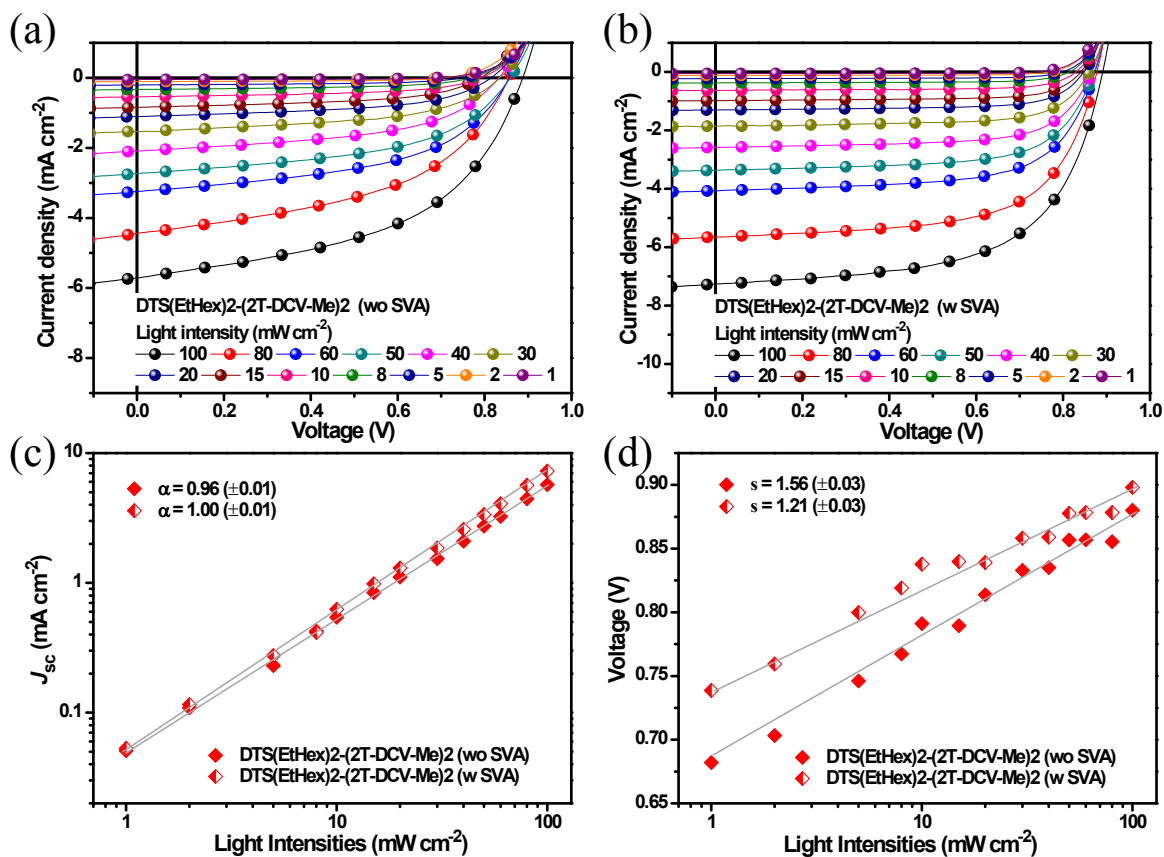


Figure S38. J - V characteristics of DTS(EtHex)₂-(2T-DCV-Me)₂:PC₇₀BM devices (a) without and (b) with SVA treatments under various light intensities ranging from 100 mW cm⁻² to 1 mW cm⁻². The measured (c) J_{sc} and (d) V_{oc} of DTS(2-EtHex)₂-(2T-DCV-Me)₂:PC₇₀BM devices with and without SVA treatments as a function of illumination intensity, together with linear fits to the relative data (solid lines).

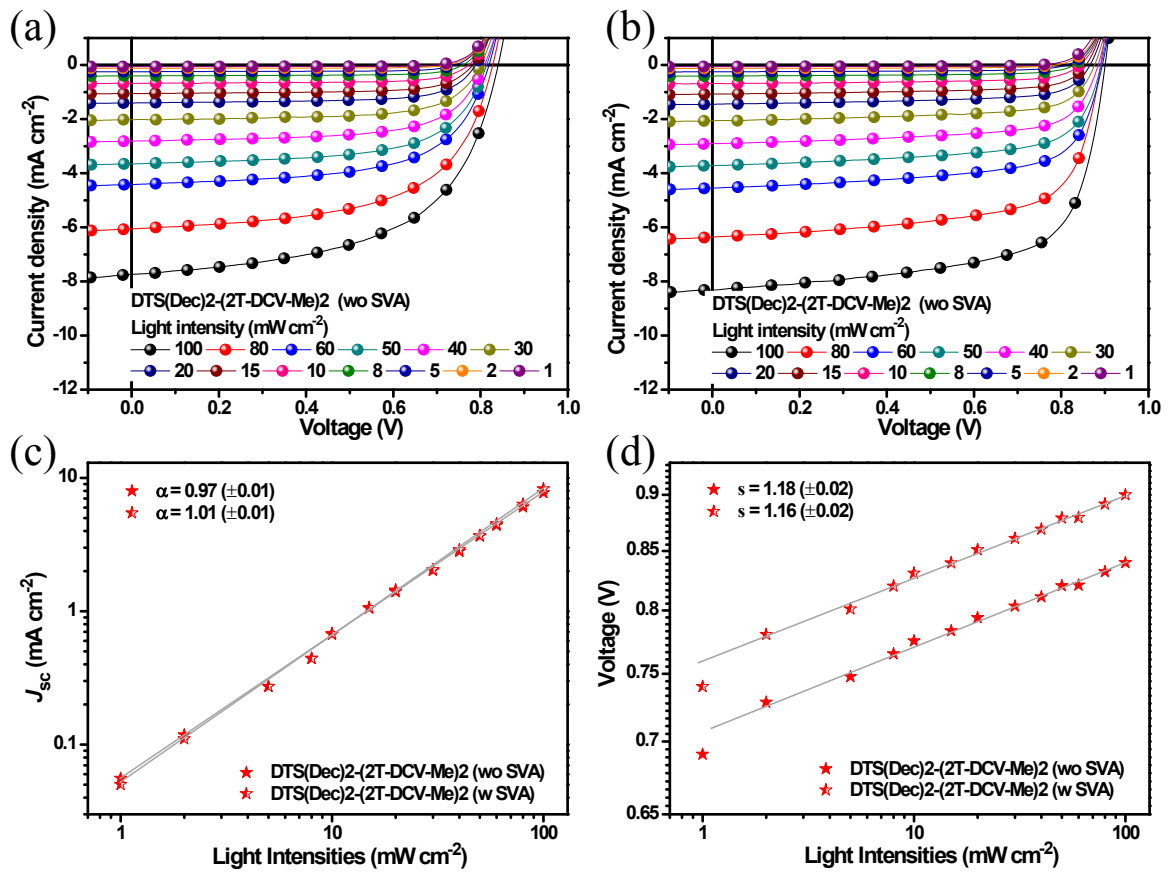


Figure S39. J - V characteristics of DTS(Dec)₂-(2T-DCV-Me)₂:PC₇₀BM devices (a) without and (b) with SVA treatments under various light intensities ranging from 100 mW cm⁻² to 1 mW cm⁻². The measured (c) J_{sc} and (d) V_{oc} of DTS(Dec)₂-(2T-DCV-Me)₂:PC₇₀BM devices with and without SVA treatments as a function of illumination intensity, together with linear fits to the relative data (solid lines).

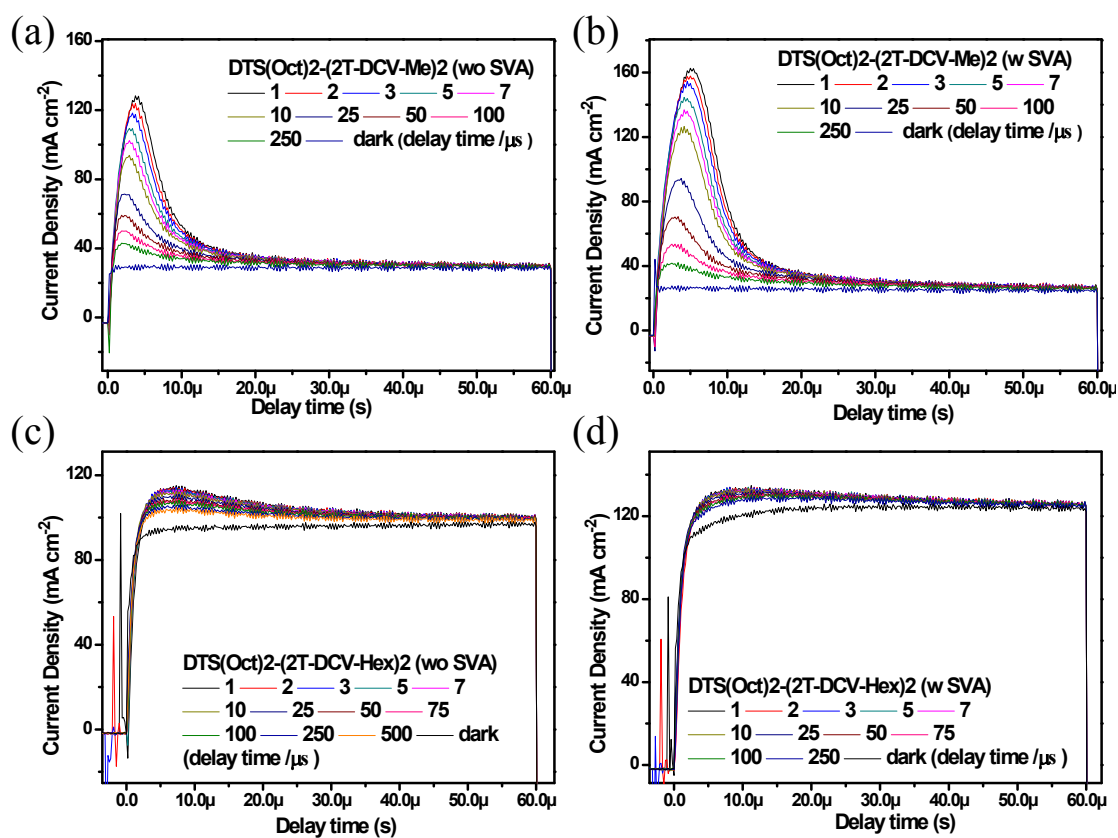


Figure S40. Photo-CELIV measurements on the DTS(Oct)₂-(2T-DCV-Me)₂:PC₇₀BM devices (a) without and (b) with SVA treatments as well as the DTS(Oct)₂-(2T-DCV-Hex)₂:PC₇₀BM devices (c) without and (d) with SVA treatments for different delay times between the light pulse and the extraction voltage ramp.

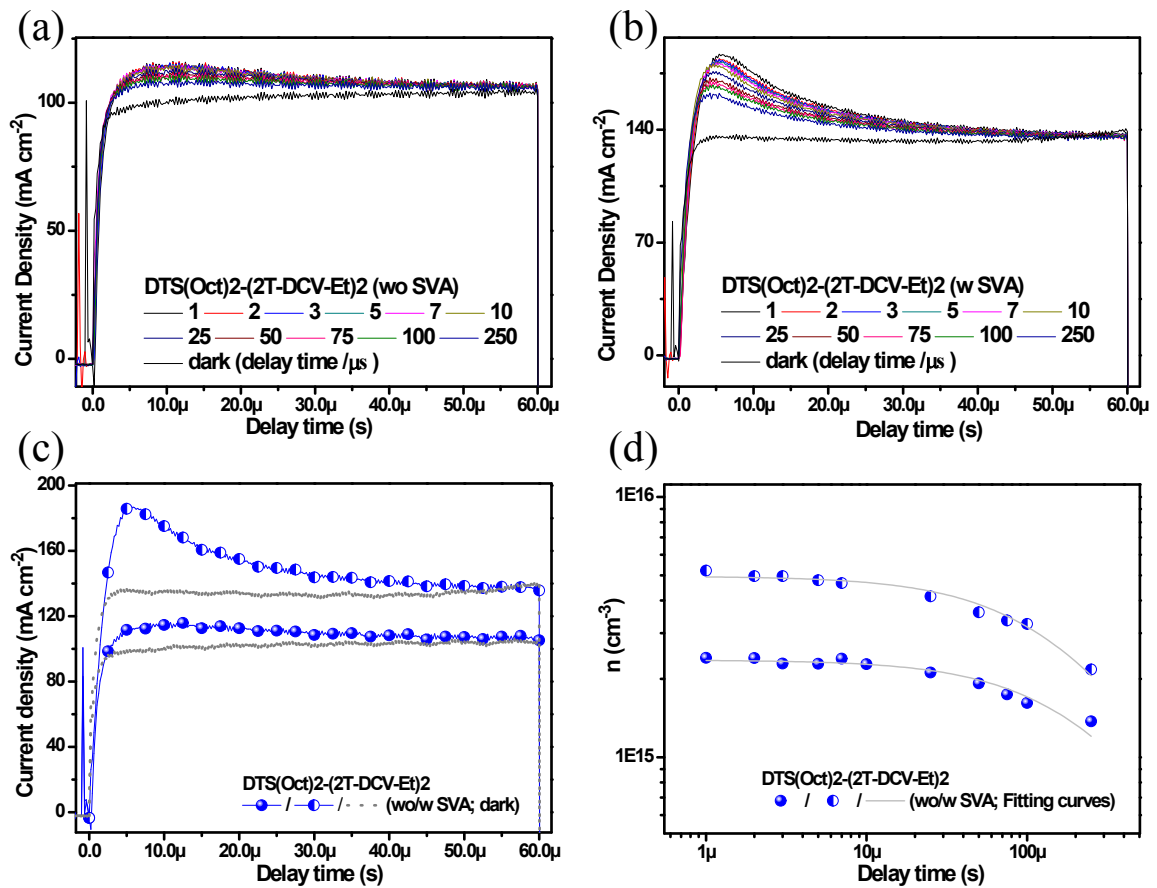


Figure S41. Photo-CELIV measurements on the DTS(Oct)₂-(2T-DCV-Me)₂:PC₇₀BM devices (a) without and (b) with SVA treatments for different delay times between the light pulse and the extraction voltage ramp. (c) The Photo-CELIV traces for the DTS(Oct)₂-(2T-DCV-Et)₂:PC₇₀BM with and without SVA treatments after a delay time of 1 μs. (d) Numbers of extracted carrier as a function of delay time and the fit.

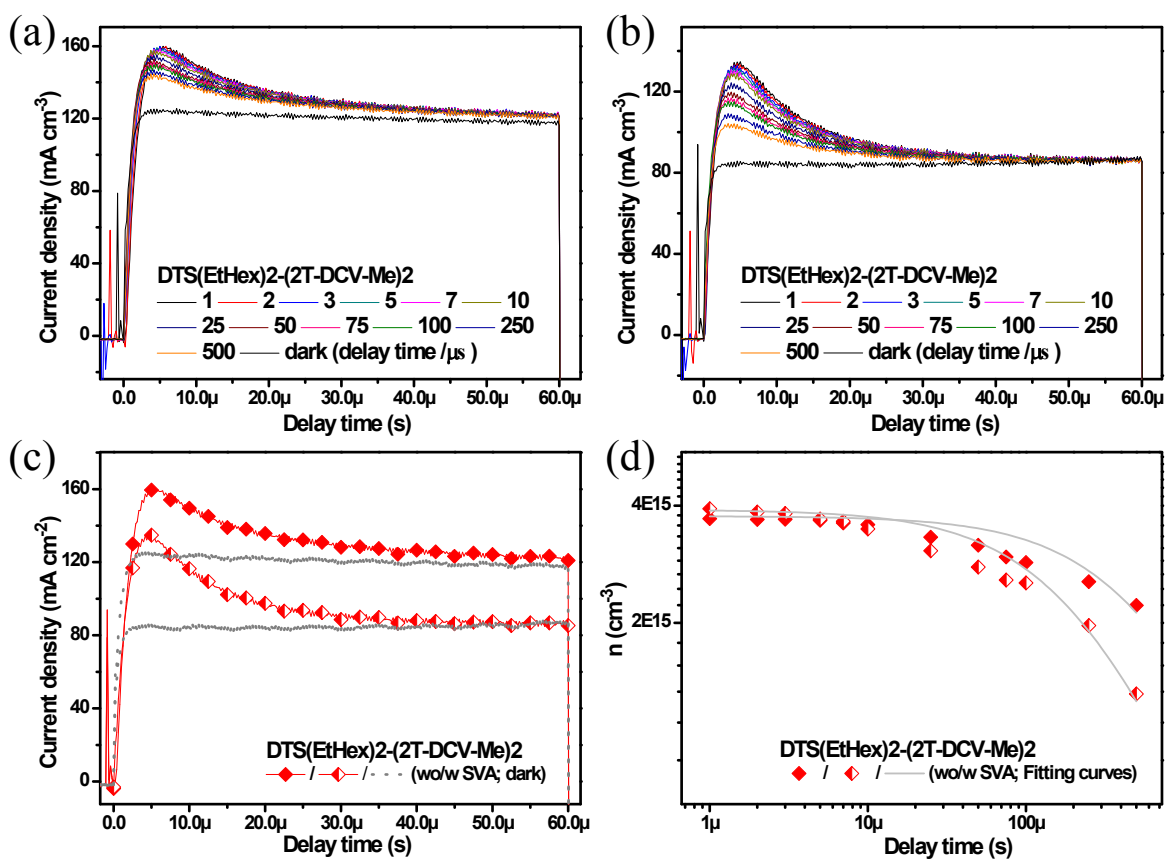


Figure S42. Photo-CELIV measurements on the DTS(EtHex)₂-(2T-DCV-Me)₂:PC₇₀BM devices (a) without and (b) with SVA treatments for different delay times between the light pulse and the extraction voltage ramp. (c) The Photo-CELIV traces for the DTS(EtHex)₂-(2T-DCV-Me)₂:PC₇₀BM with and without SVA treatments after a delay time of 1 μs. (d) Numbers of extracted carrier as a function of delay time and the fit.

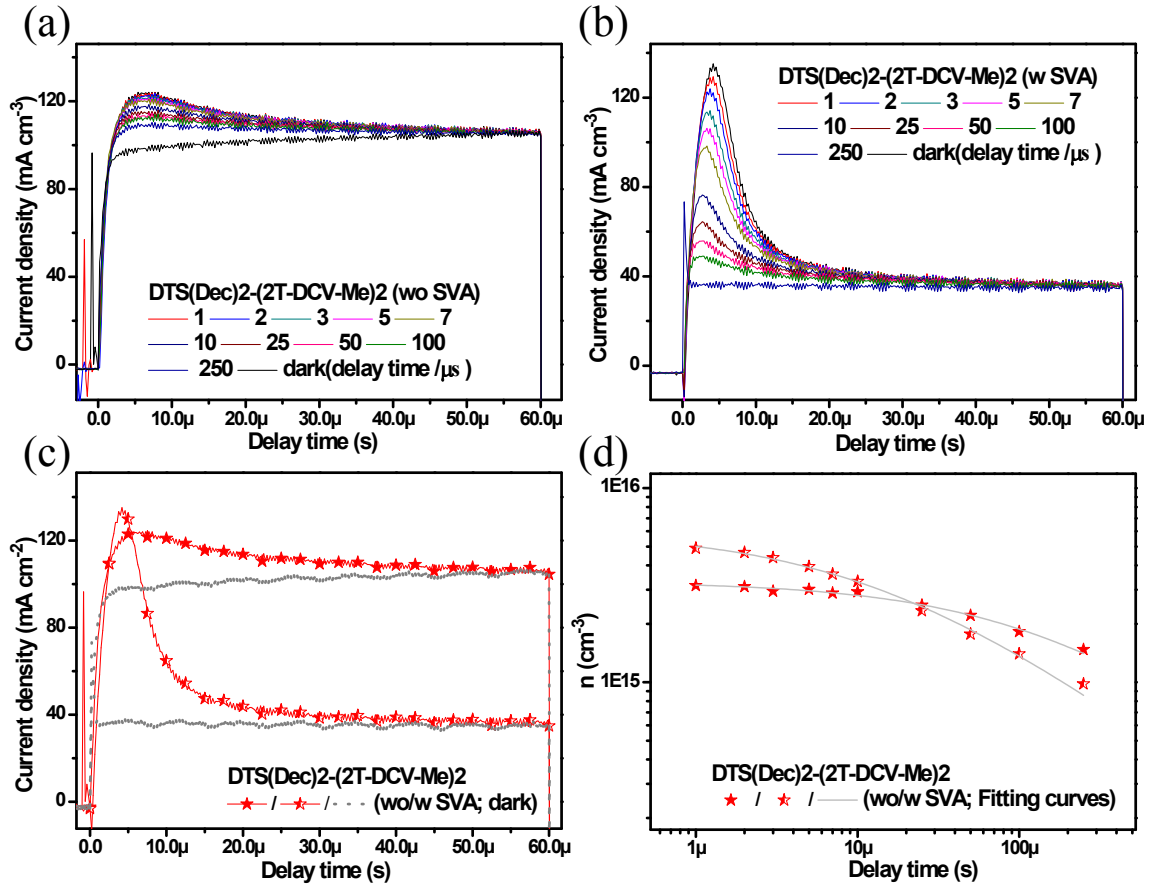


Figure S43. Photo-CELIV measurements on the DTS(Dec)₂-(2T-DCV-Me)₂:PC₇₀BM devices (a) without and (b) with SVA treatments for different delay times between the light pulse and the extraction voltage ramp. (c) The Photo-CELIV traces for the DTS(Dec)₂-(2T-DCV-Me)₂:PC₇₀BM with and without SVA treatments after a delay time of 1 μ s. (d) Numbers of extracted carrier as a function of delay time and the fit.

Table S5. Parameters extracted from Photo-CELIV signals within these two systems.

Donors	SVA treatments	μ [$\text{cm}^2\text{V}^{-1}\text{s}^{-1}$]	n_0 (cm^{-3})	τ_B [s]	t_{tr} [s]	β_L [cm^3s^{-1}]
- Oct-Me	WO	6.35×10^{-5}	7.80×10^{15}	2.71×10^{-5}	3.15×10^{-7}	4.25×10^{-11}
- Oct-Me	W	1.06×10^{-4}	2.39×10^{16}	2.48×10^{-5}	1.88×10^{-7}	7.10×10^{-11}
-Oct-Et	WO	1.31×10^{-5}	2.36×10^{15}	2.60×10^{-4}	1.53×10^{-6}	8.77×10^{-12}
-Oct-Et	W	2.86×10^{-5}	4.96×10^{15}	1.78×10^{-4}	6.99×10^{-7}	1.92×10^{-11}
- Oct-Hex	WO	1.67×10^{-5}	2.64×10^{15}	3.11×10^{-4}	1.20×10^{-6}	1.12×10^{-11}
- Oct-Hex	W	9.28×10^{-6}	2.52×10^{15}	3.41×10^{-4}	2.16×10^{-6}	6.21×10^{-12}
-EtHex-Me	WO	3.52×10^{-5}	3.75×10^{15}	6.48×10^{-4}	5.68×10^{-7}	2.36×10^{-11}
-EtHex-Me	W	4.38×10^{-5}	3.90×10^{15}	2.38×10^{-4}	4.56×10^{-7}	2.93×10^{-11}
-Dec-Me	WO	1.82×10^{-5}	3.05×10^{15}	1.67×10^{-4}	1.09×10^{-6}	1.22×10^{-11}
-Dec-Me	W	8.21×10^{-5}	4.82×10^{15}	2.73×10^{-5}	2.44×10^{-7}	5.50×10^{-11}

References

- [1] Y. N. Luponosov, J. Min, T. Ameri, C. J. Brabec and S. A. Ponomarenko, *Org. Electron.*, **2014**, *15*, 3800-3804.
- [2] Y.N. Luponosov, J. Min, A. V. Bakirov, P. V. Dmitryakov, S. N. Chvalun, S. M. Peregudova, T. Ameri, C. J. Brabec, S. A. Ponomarenko, *Dyes and Pigments*, **2015**, *122*, 213-223.
- [3] C.-H. Chen, C.-H. Hsieh, M. Duboscq, Y.-J. Cheng and C.-S. Hsu, *Macromolecules*, **2010**, *43*, 697-708.
- [4] J. Hou, H.-Y. Chen, S. Zhang, G. Li and Y. Yang, *J. Am. Chem. Soc.*, **2008**, *130*, 16144-16145.
- [5] L. Huo, H.-Y. Chen, J. Hou, T. L. Chen and Y. Yang, *Chem. Commun.*, **2009**, 5570-5572.
- [6] J. Min, Y. N. Luponosov, T. Ameri, A. Elschner, S. M. Peregudova, D. Baran, T. Heumüller, N. Li, F. Machui, S. Ponomarenko and C. J. Brabec, *Org. Electron.*, **2013**, *14*, 219-229.
- [7] J. Min, Y. N. Luponosov, A. Gerl, M. S. Polinskaya, S. M. Peregudova, P. V. Dmitryakov, A. V. Bakirov, M. A. Shcherbina, S. N. Chvalun, S. Grigorian, N. Kaush-Busies, S. A. Ponomarenko, T. Ameri and C. J. Brabec, *Adv. Energy Mater.*, **2014**, *4*, 1301234
- [8] Y. N. Luponosov, Jie Min, A. N. Solodukhin, A. V. Bakirov, P. V. Dmitryakov, M. A. Shcherbina, S. M. Peregudova, G.V. Cherkaev, E.A. Svidchenko, N. Kausch-Busies, T. Ameri, S. N. Chvalun, C. J. Brabec, S. A. Ponomarenko, Star-shaped D- π -A oligothiophenes with tris(2-methoxyphenyl)amine core and alkyldicyanovinyl groups: synthesis, photophysical, and photovoltaic properties, **2015**, in preparation.